View metadata, citation and similar papers at core.ac.uk
brought to you by CORE
provided by NASA Technical Reports Server

NASA MEMO 12-31-58A

NASA

MEMORANDUM

EXPLORATORY INVESTIGATION OF THE EFFECTS OF BOUNDARY-LAYER CONTROL ON THE PRESSURE-RECOVERY CHARACTERISTICS OF A CIRCULAR INTERNAL-CONTRACTION INLET WITH TRANSLATING CENTERBODY AT MACH NUMBERS OF 2.00 AND 2.35

By Norman J. Martin

Ames Research Center
Moffett Field, Calif.

NATIONAL AERONAUTICS AND SPACE ADMINISTRATION
WASHINGTON
February 1959
Declassified December 8, 1961

NATIONAL AERONAUTICS AND SPACE ADMINISTRATION

MEMORANDUM 12-31-58A

EXPLORATORY INVESTIGATION OF THE EFFECTS OF BOUNDARY-LAYER CONTROL ON THE PRESSURE-RECOVERY CHARACTERISTICS OF A CIRCULAR INTERNAL-CONTRACTION INLET WITH TRANSLATING CENTERBODY AT MACH NUMBERS OF 2.00 AND 2.35

By Norman J. Martin

SUMMARY

Exploratory tests of a circular internal-contraction inlet were made at Mach numbers of 2.00 and 2.35 to determine the effect of a cowl-type boundary-layer control located downstream of the inlet throat. The inlet was designed for a Mach number of 2.5. Tests were also made of the inlet modified to correspond to design Mach numbers of 2.35 and 2.25.

Surveys near the minimum area section of the inlet without boundary-layer control indicated maximum averaged pressure recoveries between 0.90 and 0.92 at a free-stream Mach number, M_∞, of 2.35 for the inlets. Farther downstream, after partial subsonic diffusion, a maximum pressure recovery of 0.842 was obtained with the inlet at $M_\infty = 2.35$. The pressure recovery of the inlet was increased by 0.03 at a Mach number of 2.35 and decreased by 0.02 at a Mach number of 2.00 by the application of cowl-type boundary-layer control. Further investigation with the inlet without bleed demonstrated that an increase of angle of attack from 0° to 3° reduced the pressure recovery 0.04. The effect of Reynolds number was to increase pressure recovery 0.07 (from 0.785 to 0.855) with an increase in Reynolds number (based on inlet diameter) from 0.79×10^6 to 3.19×10^6.

INTRODUCTION

It has been suggested by several investigators (refs. 1, 2, and 3) that high pressure recovery could be obtained with internal-compression inlets at supersonic speeds without the high wave drag associated with external-compression inlets. References 2, 3, and 4 have reported from investigation in an 8- by 8-inch wind tunnel that circular internal-compression inlets with translating centerbodies can attain pressure recoveries as good as, or slightly better than, single cone inlets up to a Mach number of 3.0 at 0° angle of attack. The effects of Reynolds

number, angle of attack, and boundary-layer control on the pressure recovery of these internal-compression type inlets were not investigated.

Since boundary-layer growth can have a large effect on the pressure-recovery characteristics of internal-compression inlets, it is desirable to determine the effect of boundary-layer control. The results of an investigation of the effect of some likely arrangements of boundary-layer control have been reported in reference 5. Presented and discussed herein are the results of an investigation in the 9- by 7-foot supersonic test section of the Unitary Plan wind tunnel of another arrangement of boundary-layer control on a similar internal-compression inlet and modifications to this inlet. In addition, there are presented the results of limited tests made to determine the effect of angle of attack (from 0° to 9°) and Reynolds number (from 0.79×10^6 to 3.5×10^6) on the pressure-recovery characteristics of these inlets.

SYMBOLS

A_1	area at station 1 without the centerbody, sq in.
$\frac{A_{min}}{A_1}$	contraction ratio (for a given centerbody position, the minimum internal area of the inlet divided by the inlet entrance area without centerbody)
$\frac{A_{local}}{A_1}$	ratio of the local duct area to the inlet entrance area
h	altitude, ft
M	Mach number
m	mass flow, lb/sec
$\frac{m_b}{m_1}$	ratio of mass flow through bleed duct to mass flow through inlet entrance for free-stream conditions
p	static pressure, lb/sq ft
p_t	total pressure, lb/sq ft
$\frac{p_l}{p_{t_\infty}}$	ratio of the local static pressure to the free-stream total pressure

$\frac{p_{t_2}}{p_{t_\infty}}$ the maximum average total-pressure recovery at station 2 for a given contraction ratio

$\frac{p_{t_3}}{p_{t_\infty}}$ the maximum area-weighted total-pressure recovery at station 3 for a given contraction ratio

$\left(\frac{p_{t_l}}{p_{t_\infty}}\right)_2$ ratio of local total pressure at station 2 to free-stream total pressure

$\left(\frac{p_{t_l}}{p_{t_\infty}}\right)_3$ ratio of local total pressure at station 3 to free-stream total pressure

r inlet entrance radius, in.

r_a local internal radius of cowl, in. (see fig. 4)

r_b local internal radius of bleed annulus, in. (see fig. 4)

r_c local radius of centerbody, in. (see fig. 4)

R Reynolds number (based on inlet diameter)

x longitudinal distance from inlet lip station (positive direction downstream), in.

$\frac{x}{r}$ longitudinal distance from the inlet lip station divided by inlet entrance radius

y radial distance from cowl internal surface, in.

α angle of attack, deg

Subscripts

av average

max maximum

min	minimum
throat	minimum area of duct
∞	free-stream condition
1	lip leading-edge station (x=0)
2	rake station 2 (x=14.547 in.)
3	rake station 3 (x=27.347 in.)
rake	compressor entrance station for inlet models of reference 4

DESCRIPTION OF MODELS

The inlet model was mounted on a body which, in turn, was sting-mounted in the wind tunnel. Figure 1 is a photograph of one of the models mounted in the tunnel. A schematic drawing of an inlet assembly is shown in figure 2. The air flow through the inlet and through the boundary-layer bleed was adjusted by remotely controlled, motor-driven plugs at the model base. The model was instrumented with 18 total-pressure tubes and 3 static-pressure tubes at duct station 3. A sketch of this rake is shown in figure 3. In addition, the cowl inner lower surface was instrumented with 20 flush static-pressure orifices in the plane of the vertical center line to determine the inlet longitudinal static-pressure distributions from the inlet lip to a point just aft of the leading edge of the cowl bleed lip. The total-pressure distribution at the throat station (duct station 2) was measured for a limited number of tests by a rake of 7 total-pressure tubes.

Sketches showing the dimensions and details of the four configurations tested are presented in figure 4. Isentropic flow was assumed and the method of characteristics was used to design the internal shape of the original inlet, hereinafter referred to as M-2.50. This inlet was designed originally to operate at a free-stream Mach number of 2.50 and a throat Mach number of 1.20 with a boundary-layer displacement area of 7 percent assumed at the throat station. For part of the investigation, inlet M-2.50 was modified to obtain contraction ratios (A_{min}/A_1) corresponding to operational free-stream Mach numbers of approximately 2.35 and 2.25 for the same throat conditions. These modifications will hereinafter be designated inlet M-2.35 and inlet M-2.25, respectively. In both cases the contraction ratios were increased by simply reducing the entrance diameter and then fairing a smooth curve into the original contour as far ahead of the throat as possible. The cowl contour aft of the faired-in location was identical for all of the inlets tested.

Another modification, referred to as inlet M-2.25S, was identical to inlet M-2.25 except for the 2.5-inch-long constant-diameter section that was inserted at the maximum diameter section of the centerbody. At the condition of minimum contraction ratio, the apex of the centerbody was 4.185 inches forward of the inlet lip leading edge for inlets M-2.50, M-2.35, and M-2.25 and 6.685 inches forward of the lip leading edge for inlet M-2.25S. Small grooves near the cowl lip leading edge and the tip of the centerbody for each configuration were installed for the purpose of promoting boundary-layer transition.

The method of determining the design Mach number as presented in this report differs from that as presented in reference 4. In order to put the design Mach numbers on the same basis, the following table has been prepared to compare the two methods of specifying design Mach number:

Inlet	M-2.50	M-2.35	M-2.25	M-2.25S
A_{min}/A_1	0.419	0.482	0.520	0.520
Design M_∞ with a 7-percent boundary-layer displacement area assumed at throat station and $M_{throat} = 1.2$ (method of present report)	2.50	2.35	2.27	2.27
Design M_∞ with assumed isentropic pressure recovery and $M_{throat} = 1.0$ (method of ref. 4)	2.39	2.24	2.15	2.15

The motor-driven centerbody was remotely controlled. The contraction ratio (A_{min}/A_1) was increased to start supersonic flow in the inlet and then reduced to improve internal compression after starting. Increase of the area ratio, A_{min}/A_1, was accomplished by forward translation of the centerbody. Curves showing the longitudinal area distribution in terms of the ratio A_{local}/A_1 for several centerbody positions are shown in figure 5 for the four different inlets. The variation of contraction ratio with centerbody position is shown in figure 6 for each inlet.

PROCEDURE

Range of Variables and Test Procedure

Tests were conducted at Mach numbers of 2.00 and 2.35 at approximate Reynolds numbers of 1.8×10^6 and 1.6×10^6, respectively. Additional tests

were conducted at a Mach number of 2.35 and Reynolds numbers of approximately 0.8×10^6 and 3.2×10^6. The angle of attack was held constant at 0° except for a limited investigation with two of the inlets at angles of attack up to 9°. Supercritical flow was established with the plugs at the model base full open by translating the centerbody forward until the terminal shock was downstream of the throat. The minimum contraction ratio was then determined by retracting the centerbody, with plugs open, until the inlet was subcritical. The maximum recovery for any supercritical operating condition and fixed centerbody position was determined by closing the plugs at the model base until the terminal shock moved to and finally through the throat, resulting in subcritical operation. Data were taken at several plug settings. When boundary-layer bleed was applied, the procedure was to set the bleed plug for a particular bleed. flow and then to determine pressure recovery in the above-described manner.

Reduction of Data

The total-pressure orifices of the rakes at stations 2 and 3 were connected to manometer boards which were photographed at each data point. The manometer boards were arranged so that the average pressures of each rake could be measured by a pressure cell and the pressure recovery computed electronically. The results thus obtained agreed with results computed from data obtained photographically. All static-pressure results were computed from data obtained photographically.

RESULTS AND DISCUSSION

Basic Characteristics

Prior to the application of boundary-layer bleed to the inlets, the basic characteristics of the various inlets without boundary-layer bleed were established. Pressure recoveries after partial subsonic diffusion (duct station 3) as a function of contraction ratio are shown in figure 7. Only the maximum pressure recovery obtained for each contraction ratio is presented. Inlet M-2.25 had the highest pressure recovery at a Mach number of 2.00 (0.90) and inlet M-2.50 had the highest pressure recovery at a Mach number of 2.35 (0.842). Although these pressure recoveries are higher (approximately 4 percent) than those of similar inlets reported in references 3 and 4, a quantitative comparison should be made with care because of the difference in diffusion between the minimum area station and the measuring station of the two inlets ($A_{min}/A_3 = 0.79$ for inlet M-2.50 compared to $A_{min}/A_{rake} = 0.51$ for inlet 1 of ref. 4 at $M_\infty = 2.35$

Effects of Bleed on Pressure Recovery

The effect of boundary-layer bleed on pressure recovery at duct station 3 is shown in figures 7 and 8. As shown in figure 8, the maximum increase in pressure recovery was obtained with a bleed flow of 14 percent of the inlet flow for inlet M-2.50 and 27 percent for inlet M-2.25S. As may be noted in figure 7, the application of boundary-layer bleed resulted in a 0.030 increase of maximum pressure recovery (from 0.842 to 0.872) for inlet M-2.50 and a 0.026 increase (from 0.800 to 0.826) for inlet M-2.25S at a free-stream Mach number of 2.35. These increases in pressure recovery with bleed were obtained at contraction ratios corresponding to those for maximum pressure recovery without bleed. Similar beneficial effects on pressure recovery were not obtained with bleed for inlets M-2.25 and M-2.35 at a free-stream Mach number of 2.35. However, the tests were exploratory and data were not obtained with bleed for the contraction ratio corresponding to maximum pressure recovery of these inlets at Mach number 2.35. At a Mach number of 2.0, the pressure recovery of inlets M-2.50 and M-2.35 was reduced by application of bleed; no data were obtained with the other two inlets at this Mach number.

Effects of Bleed on Rake Profiles

The results of the total-pressure surveys at station 2 are shown in figures 9 and 10 for inlets M-2.50, M-2.35, and M-2.25. Application of cowl bleed did not appreciably affect the measured pressures at station 2. Maximum pressure recoveries of 0.975 were measured in the center of the annular duct. Comparison of figures 9 and 10 shows the maximum pressure recovery in the center of the duct to be approximately 0.05 to 0.06 higher than the average for the rake. Although the rake at station 2 was located downstream of the minimum area section at the contraction ratio for maximum pressure recovery of each inlet, it should not be inferred that the terminal shock train necessarily started upstream of this rake.

Representative radial total-pressure surveys as shown by one portion of the rake at duct station 3 are presented in figure 11. These surveys indicate maximum pressure recoveries near the center of the duct of 95 percent for inlet M-2.50 and 90 percent for inlets M-2.35, M-2.25, and M-2.25S without boundary-layer control. Comparison of figure 11 and 7 shows that the difference between the maximum total-pressure ratios and the averaged total-pressure recoveries is of the order of 0.10 to 0.13 at this station as compared to 0.05 to 0.06 at station 2. The boundary-layer losses were greater along the cowl surface than along the centerbody surface. The addition of cowl boundary-layer bleed reduced the losses near the cowl surface; this was accompanied, however, by a generally adverse effect on the boundary layer on the centerbody surface. This

adverse effect was particularly noticeable with inlets M-2.35 and M-2.25. Data obtained with the other inlets (M-2.50 and M-2.25S) indicate this adverse effect would not be so pronounced for these latter two inlets if the data with bleed operating had been obtained at a contraction ratio corresponding to that for the highest pressure recovery without boundary-layer control.

Cowl Static-Pressure Distributions

The plots of axial static-pressure distribution along the cowl (fig. 12) show the static-pressure rise in the supersonic and subsonic compression portions of the inlet. The most rapid pressure rise is usually near the physical minimum section, but there is no sharply defined normal shock in the flow. Axial pressure distributions for constant centerbody positions with and without bleed are shown in figures 12(c) and 12(d). It appears that in each case there is a station forward of which there was no effect of bleed on the pressure distribution, but downstream of this station the pressure distribution was affected by bleed. As would be expected, all of the data show that the pressure distribution is very sensitive to centerbody position; the highest pressure rise did not always occur with the centerbody in the most retracted position.

Effects of Angle of Attack

The effect of angle of attack on pressure recovery at station 3 is shown in figure 13. An increase in angle of attack from 0° to 3° at a free-stream Mach number of 2.35 resulted in a decrease of 0.04 in pressure recovery for inlet M-2.50. Further increase of angle of attack from 3° to 6° resulted in an 0.01 increase in pressure recovery. At a Mach number of 2.00, the decrease with angle of attack for the angular range from 0° to 6° was only 0.025. With inlet M-2.25 there was also very little effect of angle of attack, up to 9° at a Mach number of 2.00. However, it should be noted that at $M_\infty = 2.0$ the inlets operated with supersonic spillage which tends to mask the effect of angle of attack.

The radial total-pressure distributions at rake station 3 are compared in figure 14 for three angles of attack at a Mach number of 2.35. As would be expected, an increase of angle of attack caused a large variation in these radial distributions at the different circumferential stations. However, the over-all distortion, $p_{t_{max}} - p_{t_{min}} / p_{t_{av}}$, is less at 6° than at 3° angle of attack (0.533 at 6° compared to 0.568 at 3°). A comparison of the axial static-pressure distribution along the cowl at the three angles of attack is shown in figure 15.

Effects of Reynolds Number

The effect of changing Reynolds number on pressure recovery at station 3 is shown in figure 16. The effect of Reynolds number was to increase the pressure recovery by 0.07 (from 0.785 to 0.855) and decrease the optimum contraction ratio by 0.013 (from 0.513 to 0.500) with an increase of duct Reynolds number from 0.79×10^6 to 3.19×10^6. The change in optimum contraction ratio would account for only a small portion of the change of pressure recovery. It is possible that the boundary-layer trips on the cowl and centerbody did not fix transition as was expected. The large effect of Reynolds number is believed to indicate a particular sensitivity of internal compression inlets to boundary-layer conditions. This would necessitate proper interpretation of the test data in relation to flight conditions. The flight Reynolds numbers for an inlet sized to match some typical present and future engines are presented in figure 17. It may be noted that the range of the test Reynolds numbers is similar to the range of flight Reynolds numbers at high altitudes. This similarity indicates that the present test results may be applicable to inlets designed for use with certain engines at high altitude; the results should be used with discretion if applied at lower altitudes and higher Reynolds numbers.

CONCLUDING REMARKS

Exploratory tests were made at free-stream Mach numbers of 2.35 and 2.00 of a circular internal-contraction inlet and modifications to this inlet all having a translating centerbody and a cowl-type boundary-layer bleed located downstream of the inlet throat. Although this arrangement of boundary-layer control was not considered optimum, its use on the original inlet resulted in an increase of pressure recovery of 0.03 at a Mach number of 2.35 and a decrease of 0.02 at a Mach number of 2.00.

Investigation of the best inlet configuration without bleed at a free-stream Mach number of 2.35 revealed that the pressure recovery was reduced a maximum of 0.04 by an increase of angle of attack from 0° to 3°. This loss in pressure recovery was accompanied by an increase in flow distortion. Further increase of angle of attack from 3° to 6° resulted in an 0.01 increase of pressure recovery. The pressure recovery of the same inlet was increased 0.07 with an increase of duct Reynolds number (based on inlet diameter) from 0.79×10^6 to 3.5×10^6.

Ames Research Center
National Aeronautics and Space Administration
Moffett Field, Calif., Aug. 27, 1958

REFERENCES

1. Ferri, Antonio, and Nucci, Louis M.: Theoretical and Experimental Analysis of Low-Drag Supersonic Inlets Having a Circular Cross Section and a Central Body at Mach Numbers of 3.30, 2.75, and 2.45. NACA Rep. 1189, 1954 (Supersedes NACA RM L8H13).

2. Mossman, Emmet A., and Pfyl, Frank A.: A Study of a Symmetrical, Circular, Internal Compression Inlet. NACA RM A55L16, 1956.

3. Mossman, Emmet A., Pfyl, Frank A., and Lazzeroni, Frank A.: Fuselage Side Inlets - A Study of Some Factors Affecting Their Performance and a Comparison With Nose Inlets. NACA RM A55F29, 1956.

4. Mossman, Emmet A., and Pfyl, Frank A.: An Experimental Investigation at Mach Numbers From 2.1 to 3.0 of Circular-Internal-Contraction Inlets With Translating Centerbodies. NACA RM A56G06, 1956.

5. Bowditch, David N., and Anderson, Bernhard H.: Performance of an Isentropic, All Internal Contraction, Axisymmetric Inlet Designed For Mach Number 2.50. NACA RM E58E16, 1958.

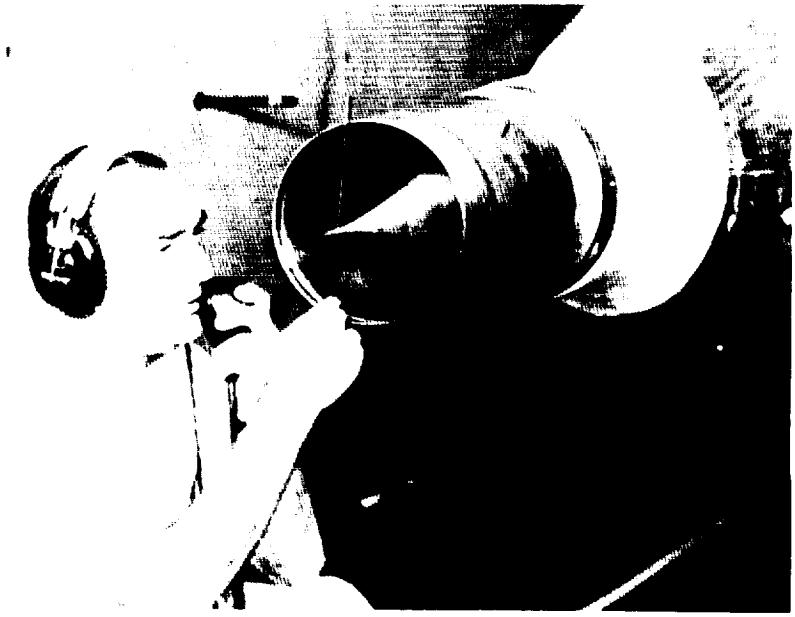

A-22896

Figure 1.- Inlet model installed in the tunnel.

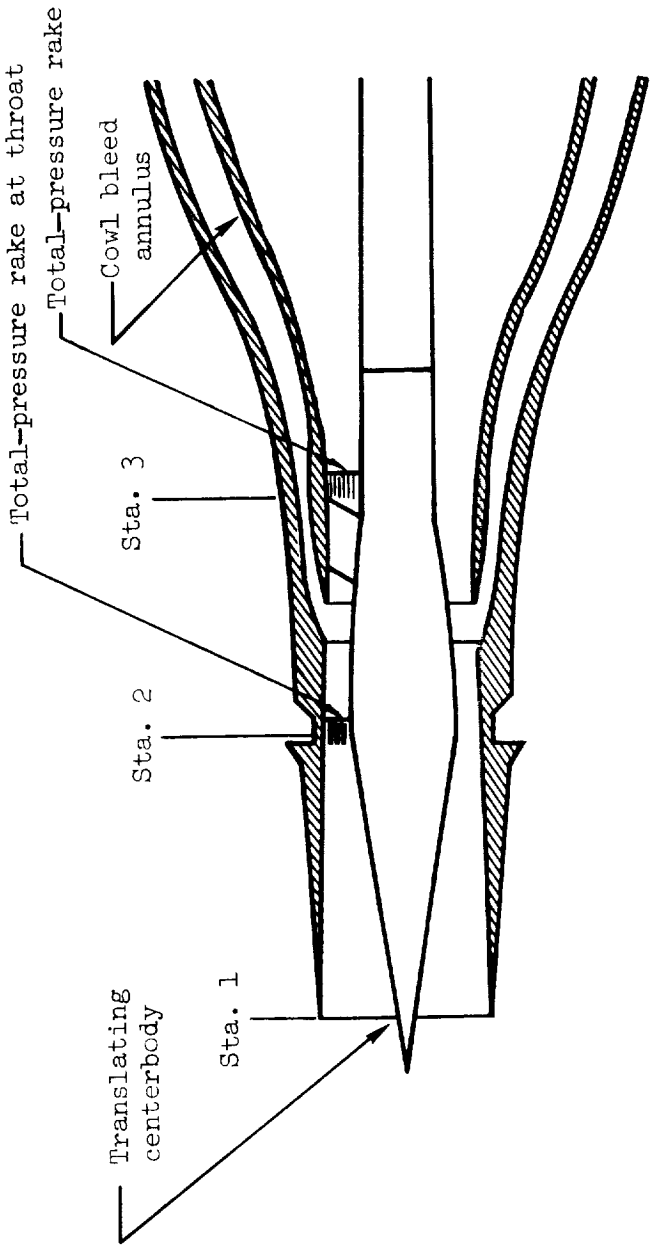

Figure 2.- Schematic drawing showing assembly of the circular internal-contraction inlets.

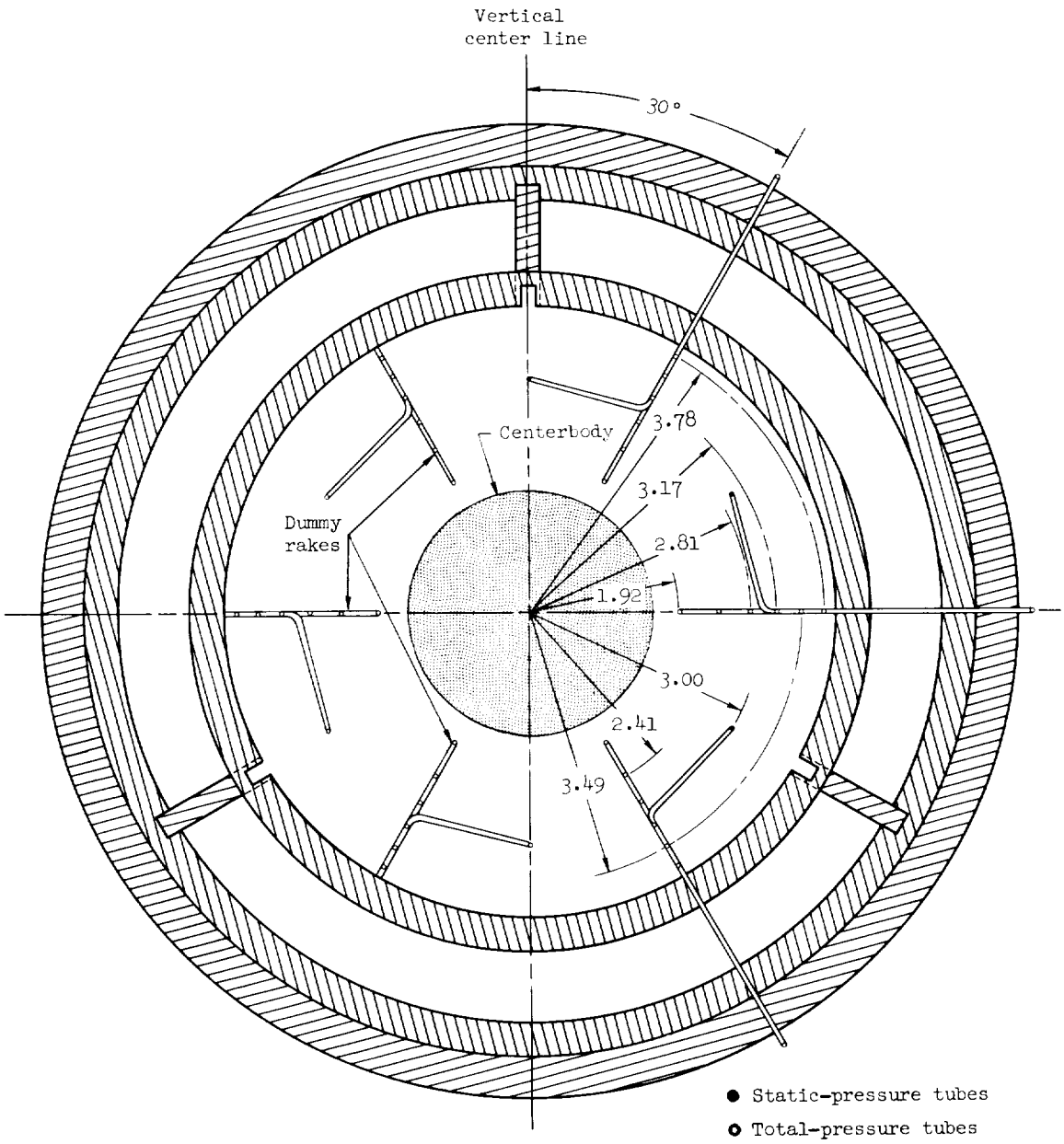

Figure 3.- Pressure measuring rake at duct station 3 (all dimensions in inches).

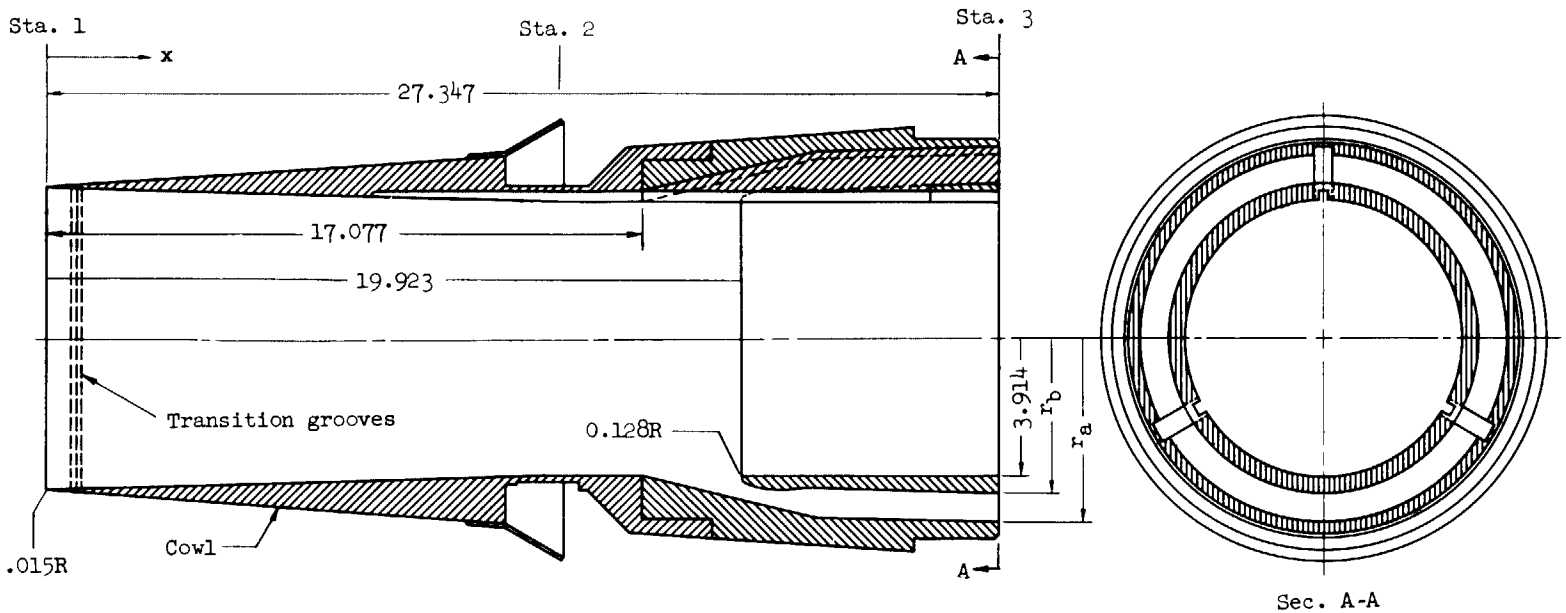

Coordinates of cowl

x	r_a	r_b	x	r_a	r_b
0	4.466		7.547	4.241	
0.547	4.466		8.547	4.178	
1.547	4.464		9.547	4.117	
2.547	4.458		10.547	4.055	
3.547	4.435		11.547	3.997	
4.547	4.401		12.547	3.952	
5.547	4.356		13.547	3.921	
6.547	4.302		14.547	3.914	

x	r_a	r_b	x	r_a	r_b
17.077	3.914		21.361	5.008	4.303
17.451	3.939		21.597	5.058	4.306
17.820	4.016		21.847	5.097	4.291
18.597	4.234		22.097	5.122	4.271
19.923	4.606	4.041	22.339	5.134	
20.067		4.172	22.429		4.259
20.647	4.810	4.230	24.847	5.205	4.328
21.175	4.961		27.347	5.280	4.400

(a) Cowl for inlet M-2.50.

Figure 4.- Sketches showing annulus and centerbody details of the four inlet configurations.

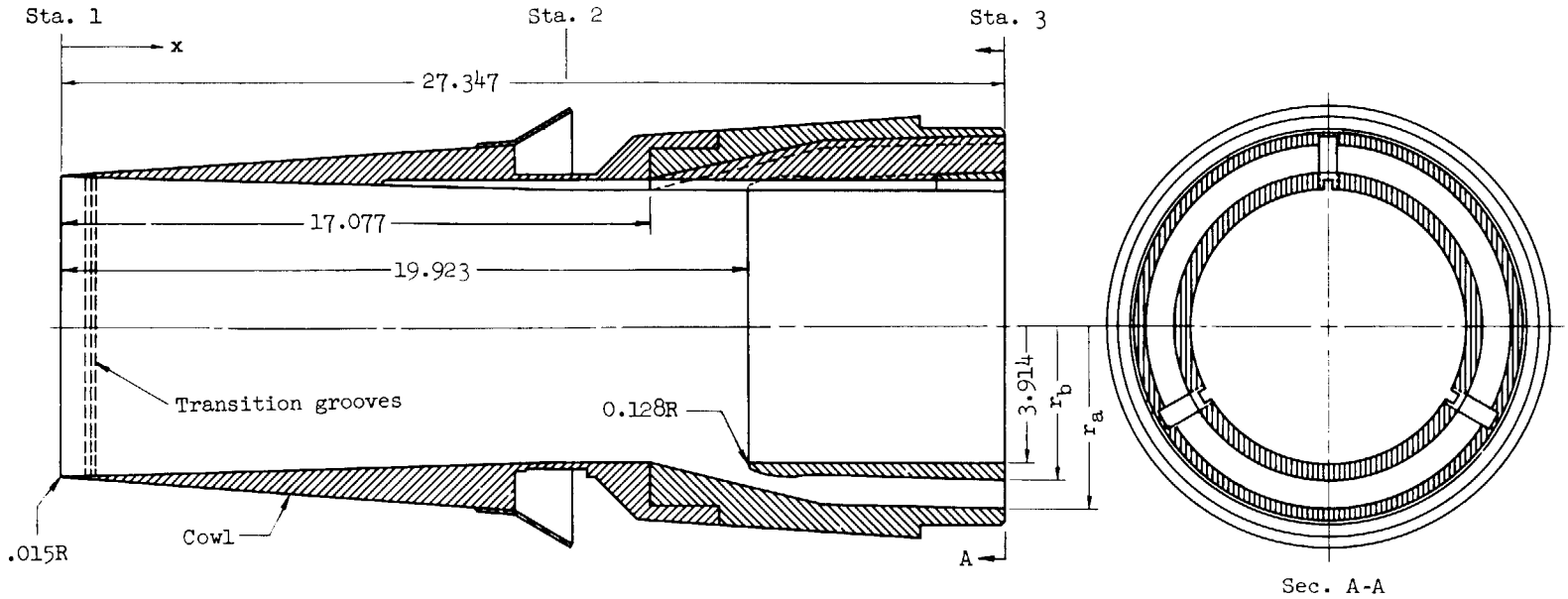

Coordinates of cowl

x	r_a	r_b	x	r_a	r_b
0	4.166		7.547	4.105	
0.547	4.166		8.547	4.087	
1.547	4.164		9.547	4.065	
2.547	4.160		10.547	4.036	
3.547	4.153		11.547	3.994	
4.547	4.144		12.547	3.952	
5.547	4.133		13.547	3.921	
6.547	4.120		14.547	3.914	

x	r_a	r_b	x	r_a	r_b
17.077	3.914		21.361	5.008	4.303
17.451	3.939		21.597	5.058	4.306
17.820	4.016		21.847	5.097	4.291
18.597	4.234		22.097	5.122	4.271
19.923	4.606	4.041	22.339	5.134	
20.067		4.172	22.429		4.259
20.647	4.810	4.230	24.847	5.205	4.328
21.175	4.961		27.347	5.280	4.400

(b) Cowl for inlet M-2.35.

Figure 4.- Continued.

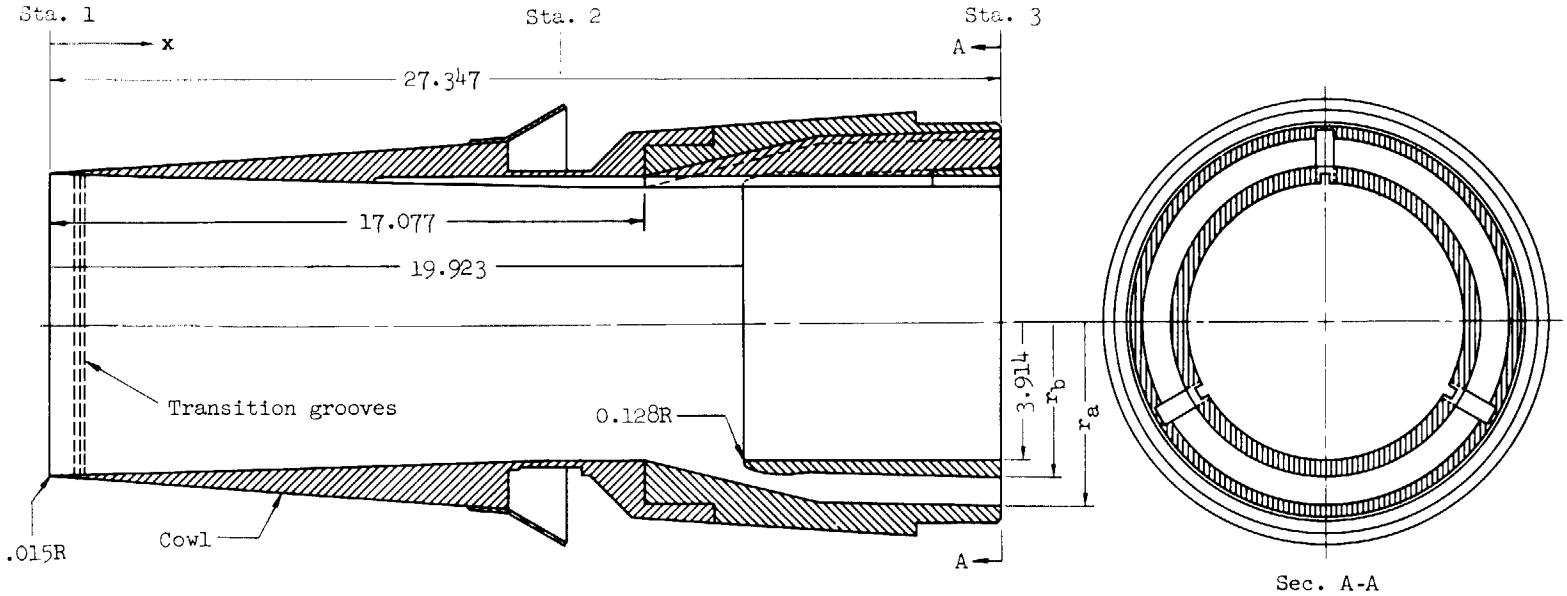

Coordinates of cowl

x	r_a	r_b	x	r_a	r_b
0	4.010		7.547	4.008	
0.547	4.010		8.547	4.004	
1.547	4.010		9.547	3.998	
2.547	4.010		10.547	3.988	
3.547	4.010		11.547	3.973	
4.547	4.010		12.547	3.952	
5.547	4.010		13.547	3.921	
6.547	4.010		14.547	3.914	

x	r_a	r_b	x	r_a	r_b
17.077	3.914		21.361	5.008	4.303
17.451	3.939		21.597	5.058	4.306
17.820	4.016		21.847	5.097	4.291
18.597	4.234		22.097	5.122	4.271
19.923	4.606	4.041	22.339	5.134	
20.067		4.172	22.429		4.259
20.647	4.810	4.230	24.847	5.205	4.328
21.175	4.961		27.347	5.280	4.400

(c) Cowl for inlets M-2.25 and M-2.25S.

Figure 4.- Continued.

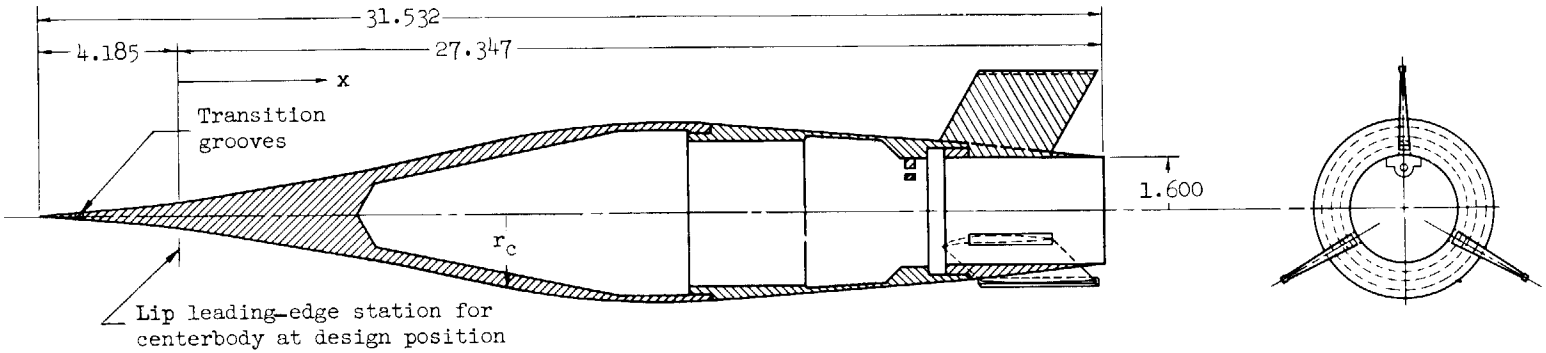

Coordinates of centerbody

x	r_c	x	r_c
-4.185	0; 5° cone to x=-3.453	2.547	0.795
		3.547	0.966
-3.453	0.033	4.547	1.142
-2.453	0.114	5.547	1.326
-1.453	0.220	6.547	1.517
-0.453	0.341	7.547	1.717
0.000	0.419	8.547	1.934
0.547	0.487	9.547	2.129
1.547	0.638	10.547	2.304

x	r_c	x	r_c
11.547	2.445	20.547	2.253
12.547	2.541	21.547	2.180
13.547	2.599	22.547	2.095
14.547	2.637	23.547	2.000
15.547	2.614	24.547	1.898
16.547	2.554	25.547	1.788
17.547	2.488	26.547	1.683
18.547	2.408	27.347	1.600
19.547	2.335		

(d) Centerbody for inlets M-2.50, M-2.35, and M-2.25.

Figure 4.- Continued.

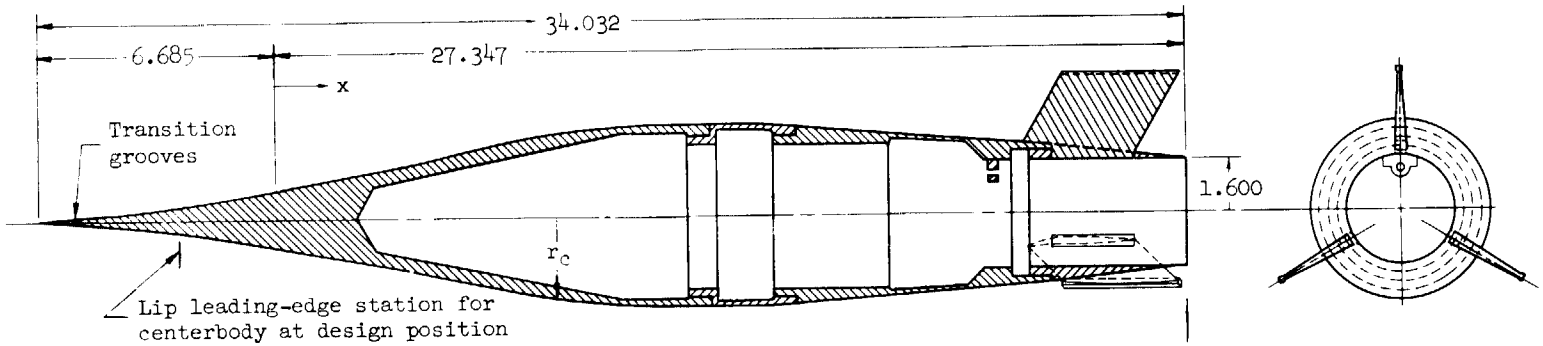

Coordinates of centerbody

x	r_c	x	r_c
-6.685	0; 5° cone	1.047	0.966
	to x=-5.953	2.047	1.142
[illegible]	[illegible]	[illegible]	[illegible]
-4.953	0.114	4.047	1.517
-3.953	0.220	5.047	1.717
-2.953	0.341	6.047	1.934
-2.500	0.419	7.047	2.129
-1.953	0.487	8.047	2.304
-0.953	0.638	9.047	2.445
0.047	0.795	10.047	2.541

x	r_c	x	r_c
11.047	2.599	20.547	2.253
12.047	2.637	21.547	2.180
[illegible]	[illegible]	[illegible]	[illegible]
14.047	2.637	23.547	2.000
14.547	2.637	24.547	1.898
15.547	2.614	25.547	1.788
16.547	2.554	26.547	1.683
17.547	2.488	27.347	1.600
18.547	2.408		
19.547	2.335		

(e) Centerbody for inlet M-2.25S.

Figure 4.- Concluded.

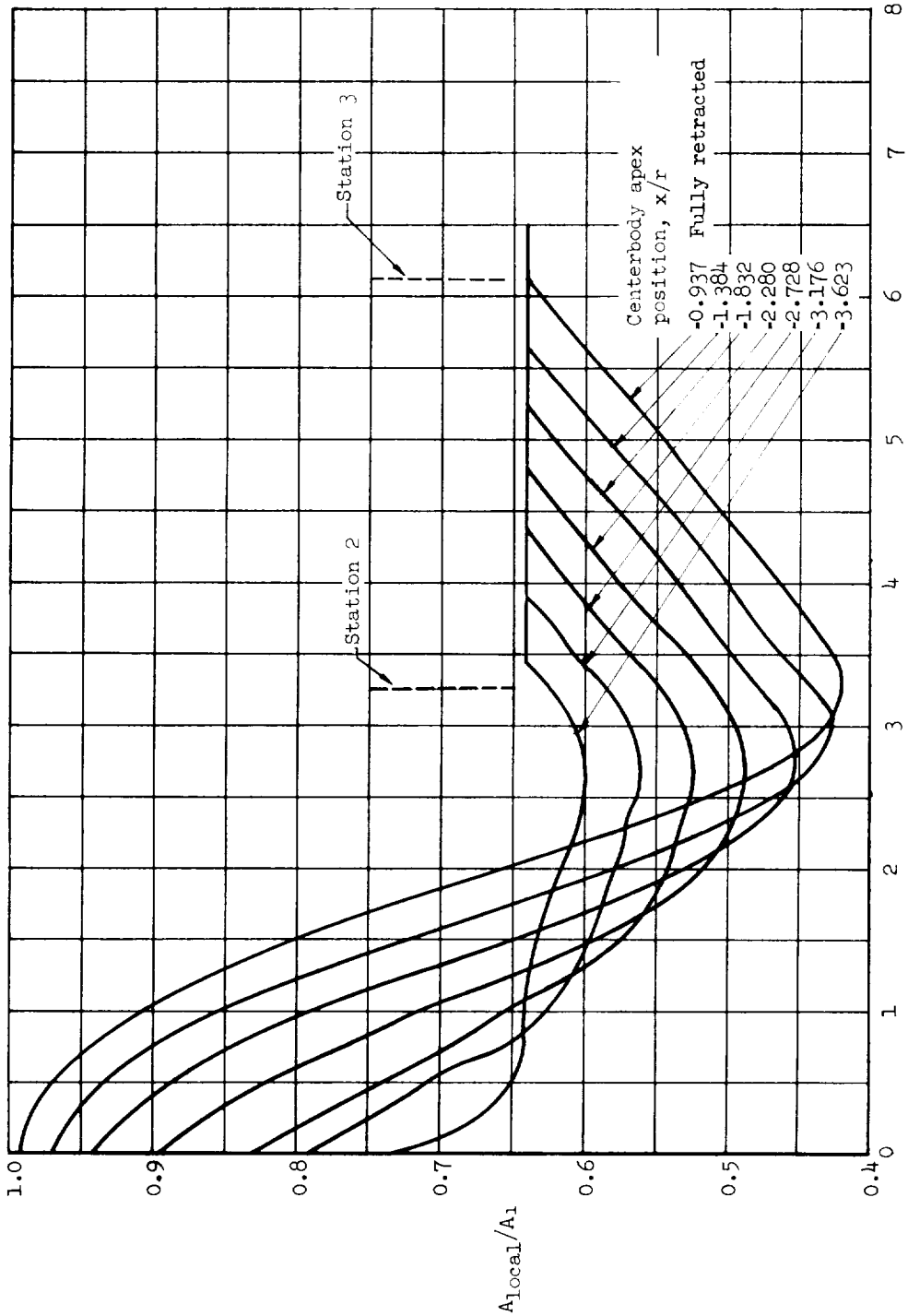

(a) Inlet M-2.50.

Figure 5.- Distribution of area ratio for inlets without bleed.

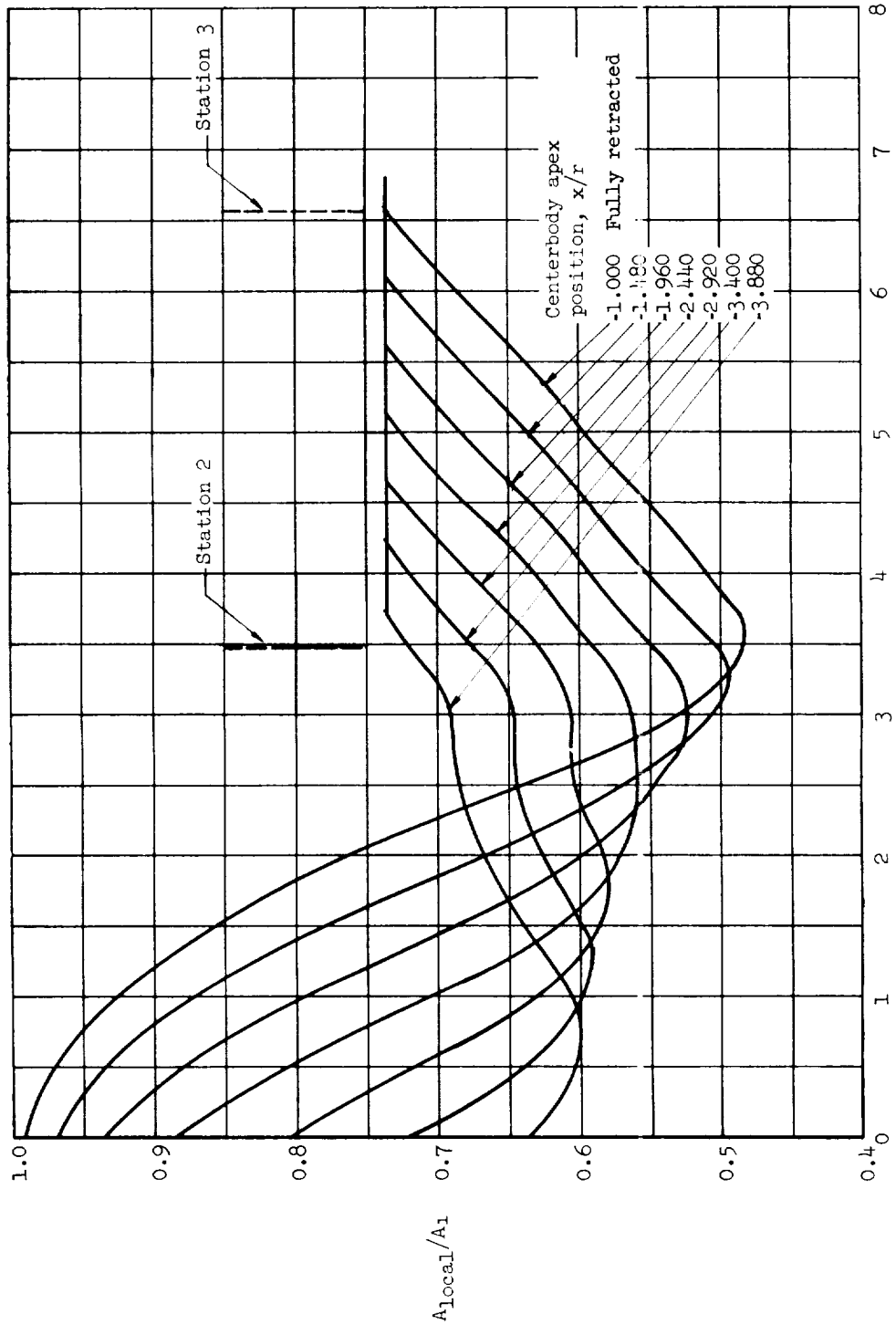

(b) Inlet M-2.35.

Figure 5.- Continued.

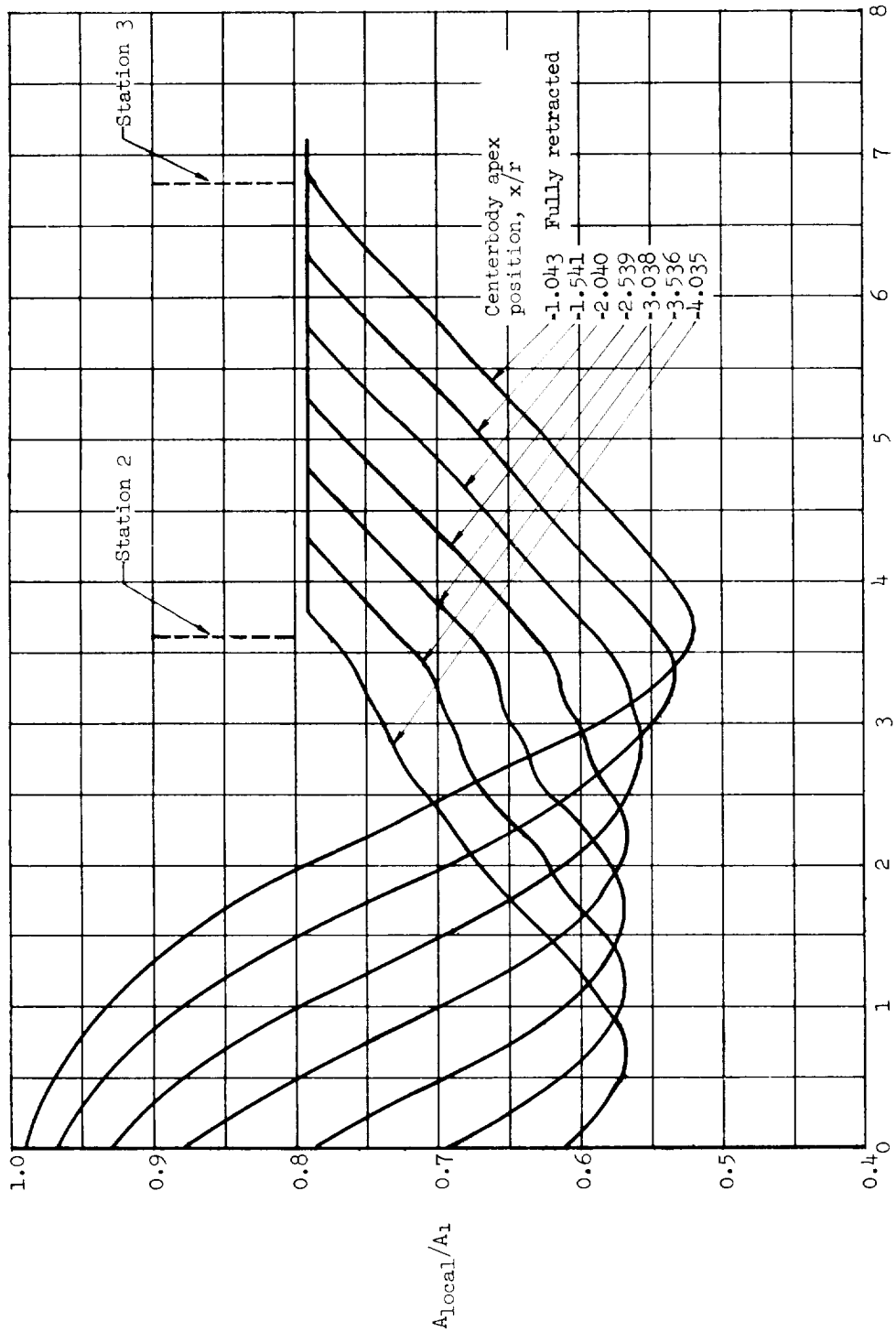

(c) Inlet M-2.25.

Figure 5.- Continued.

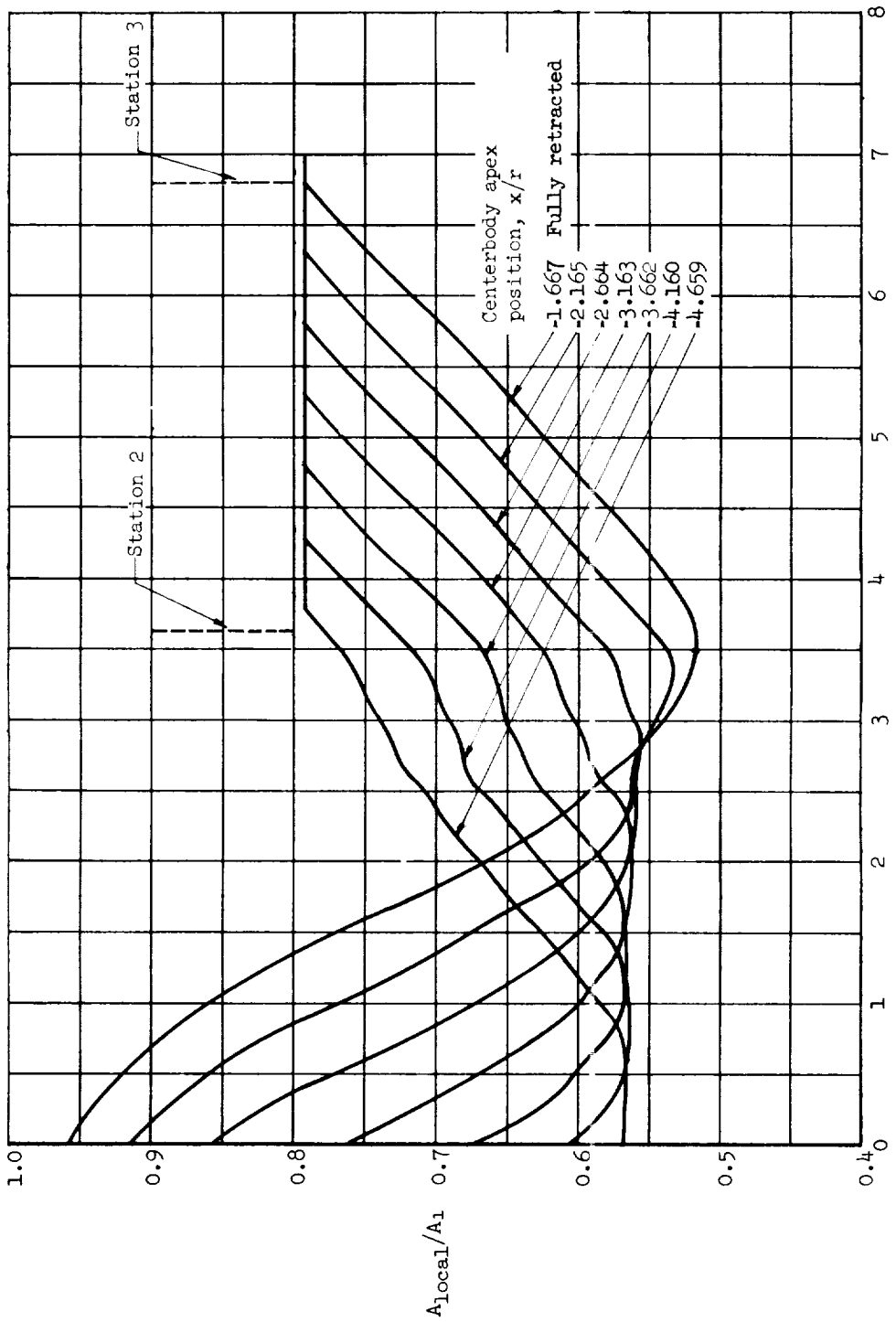

(d) Inlet M-2.25S.

Figure 5.- Concluded.

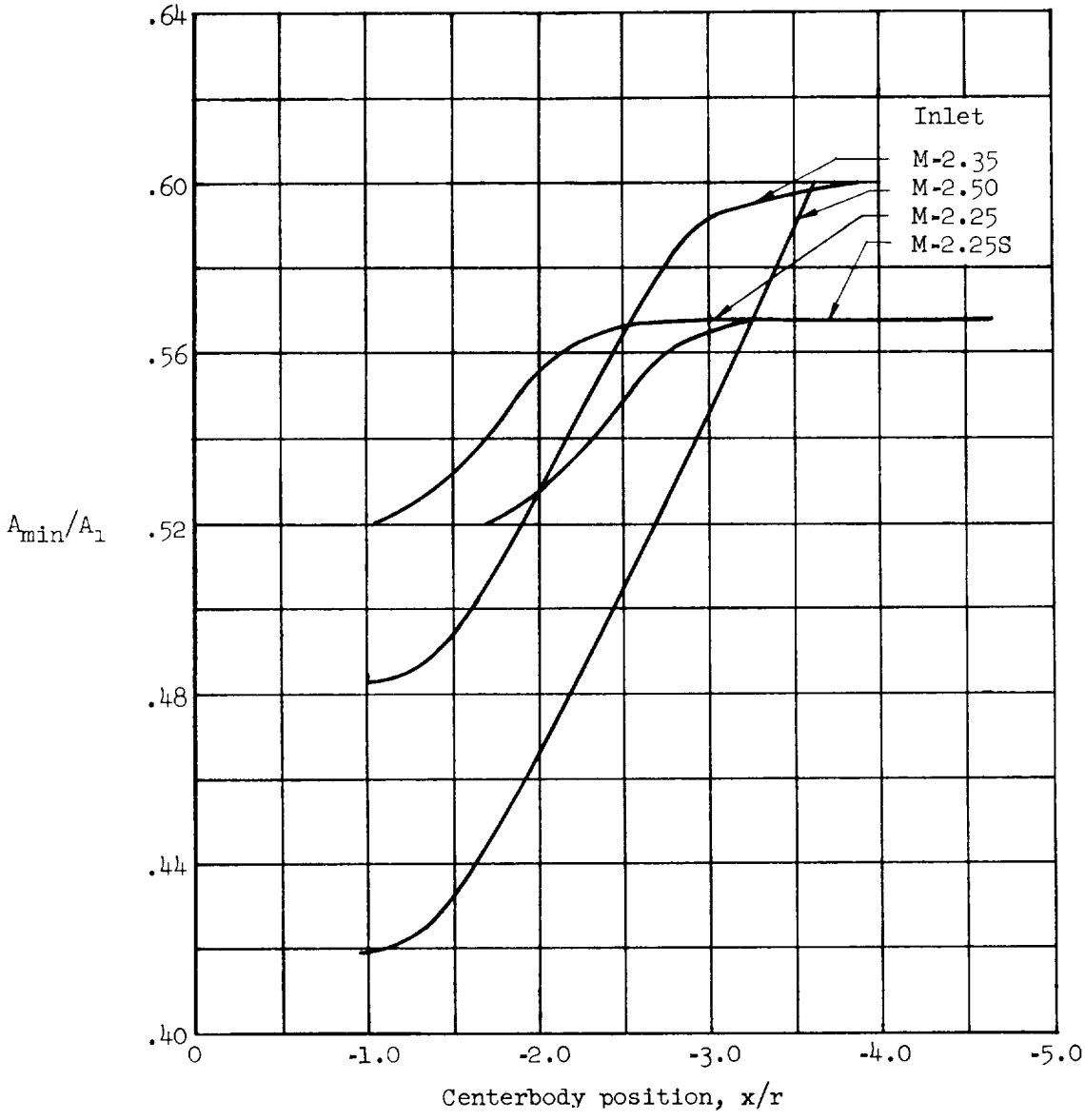

Figure 6.- Variation of contraction ratio for each inlet as a function of centerbody position.

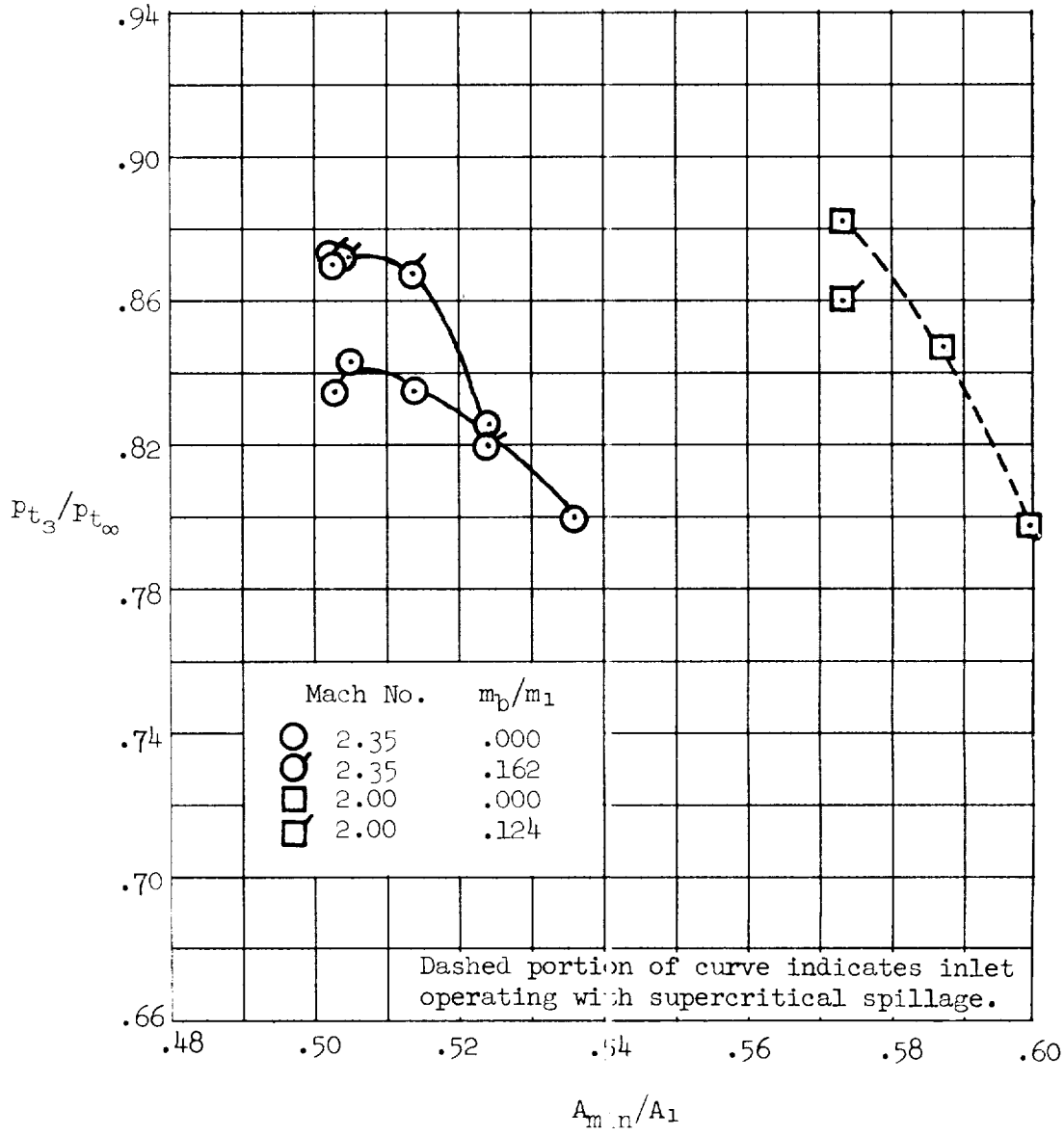

(a) Inlet M=2.50.

Figure 7.- Total-pressure recovery at duct station 3 as a function of contraction ratio; $\alpha=0^\circ$.

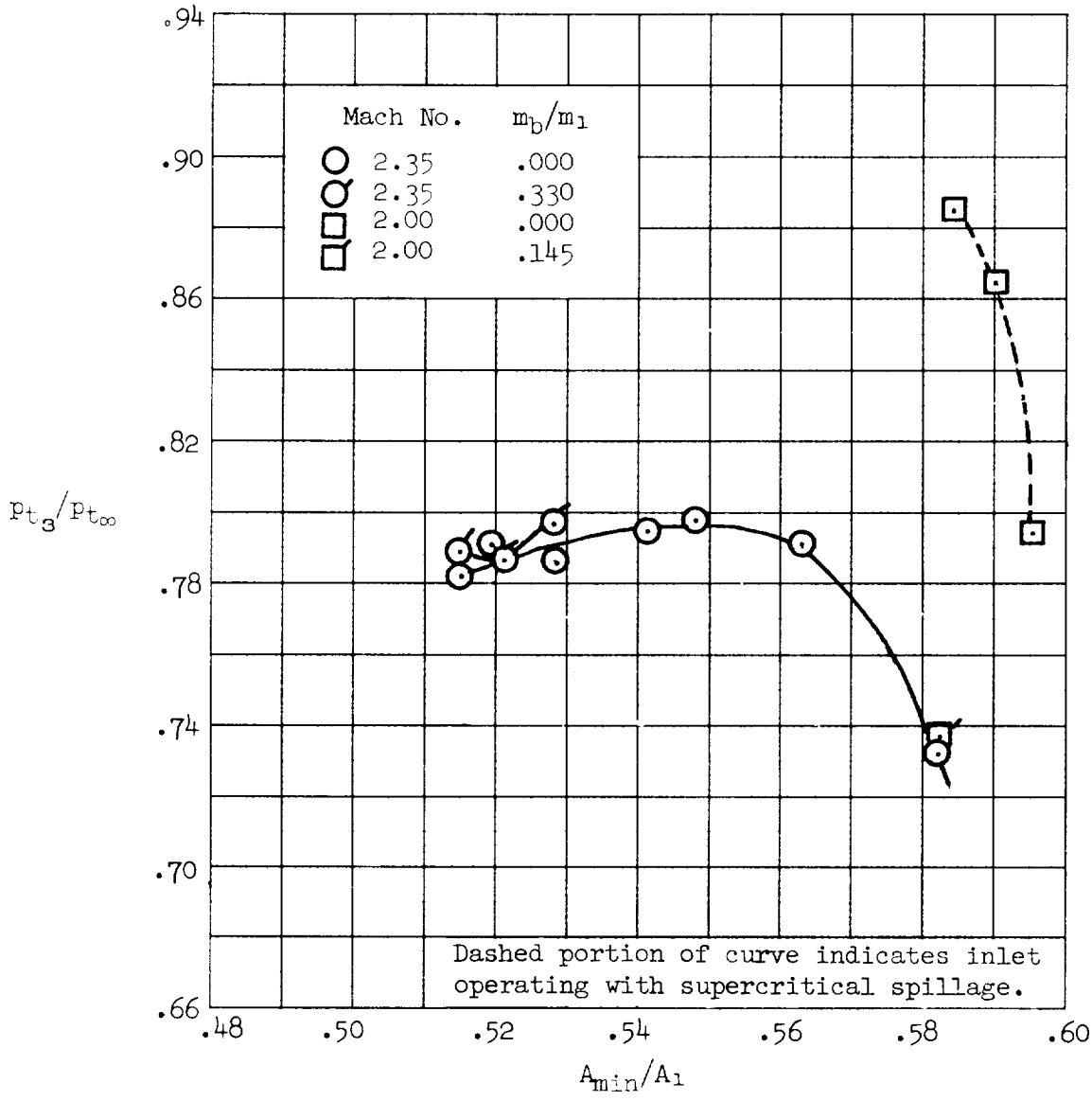

(b) Inlet M-2.35.

Figure 7.- Continued.

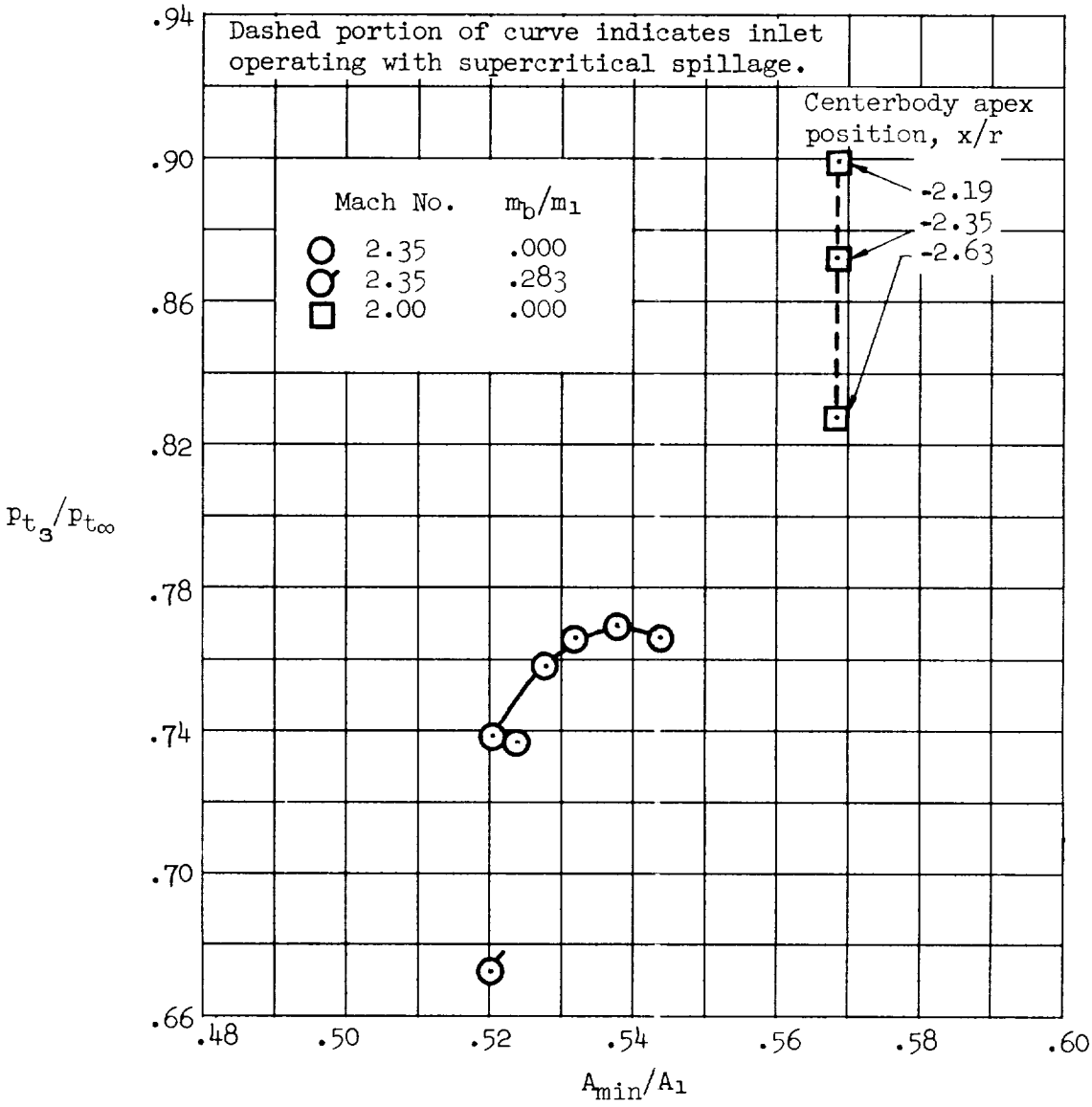

(c) Inlet M-2.25.

Figure 7.- Continued.

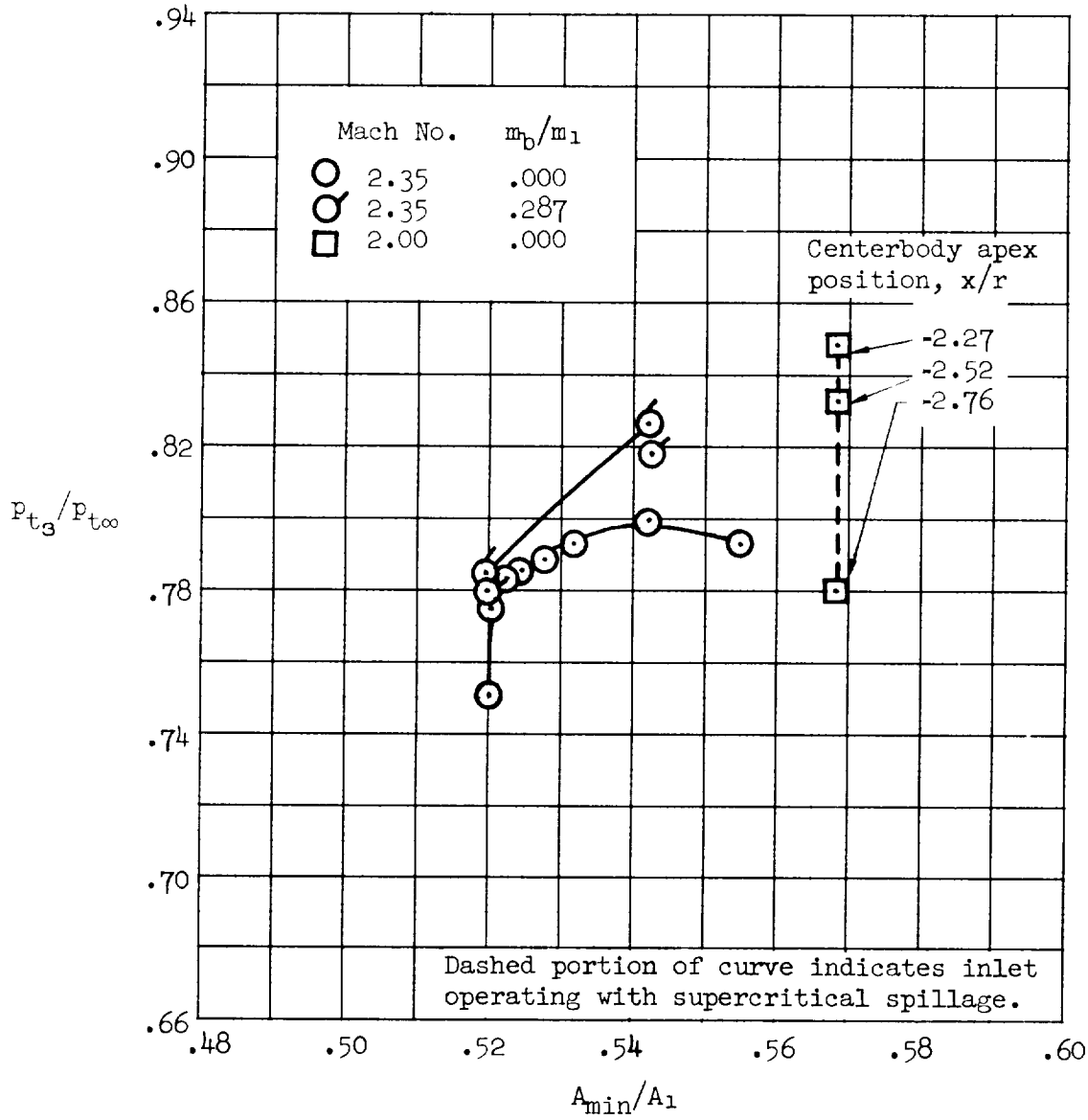

(d) Inlet M-2.25S.

Figure 7.- Concluded.

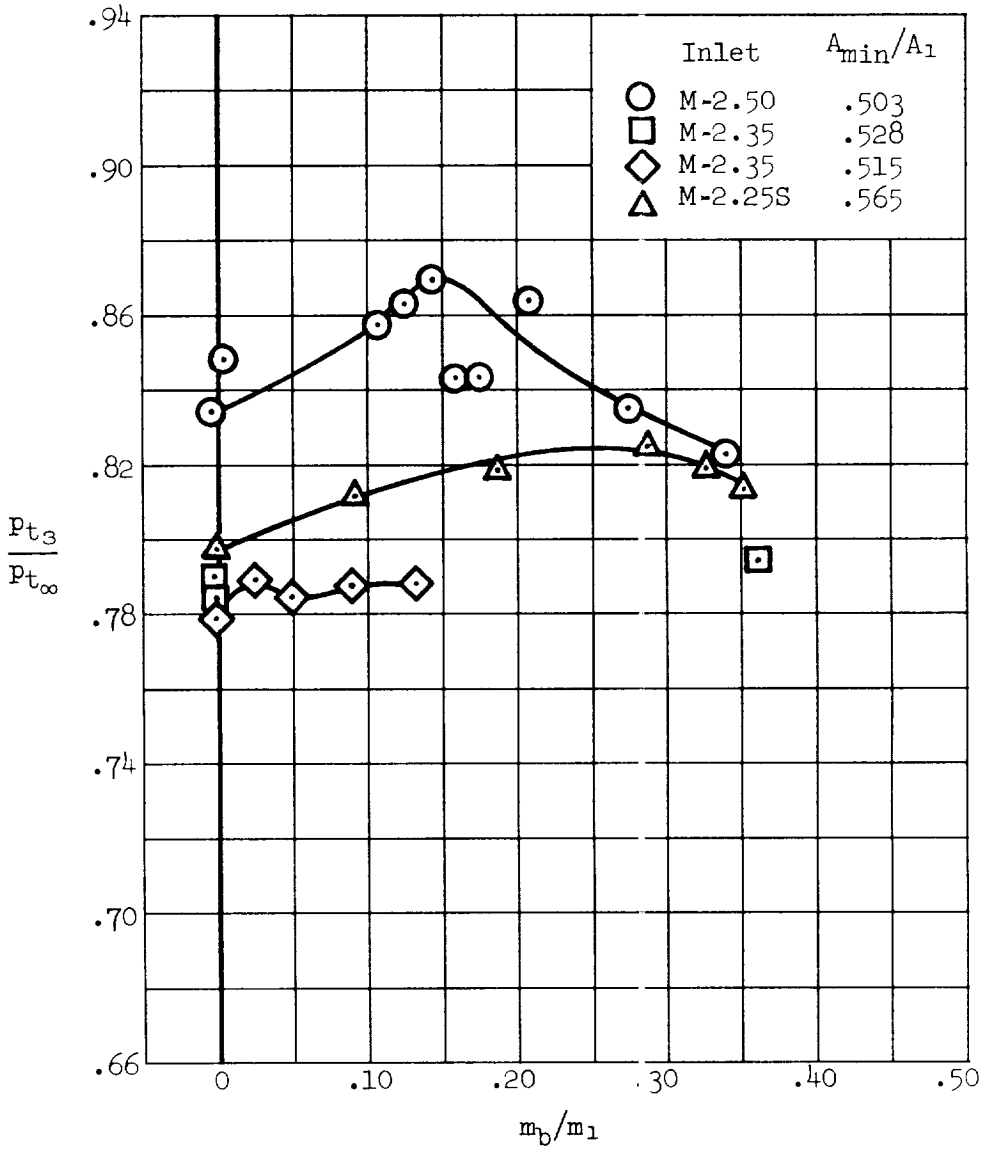

Figure 8.- Effect of the amount of cowl bleed on total-pressure recovery of the inlets at $M_\infty=2.35$; $\alpha=0^\circ$.

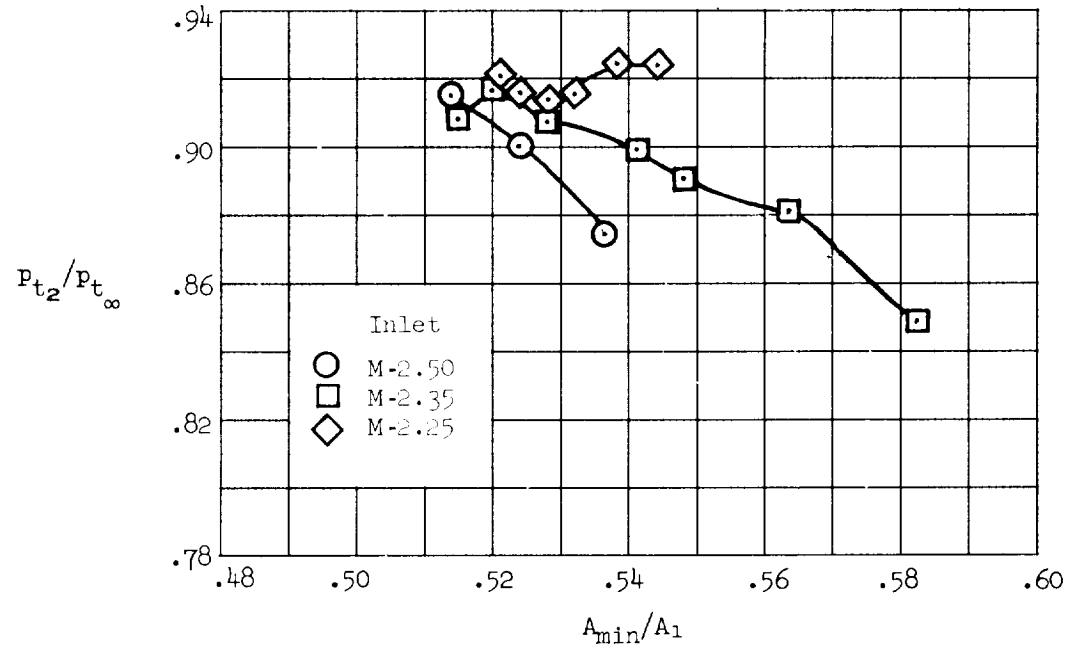

(a) No boundary-layer bleed.

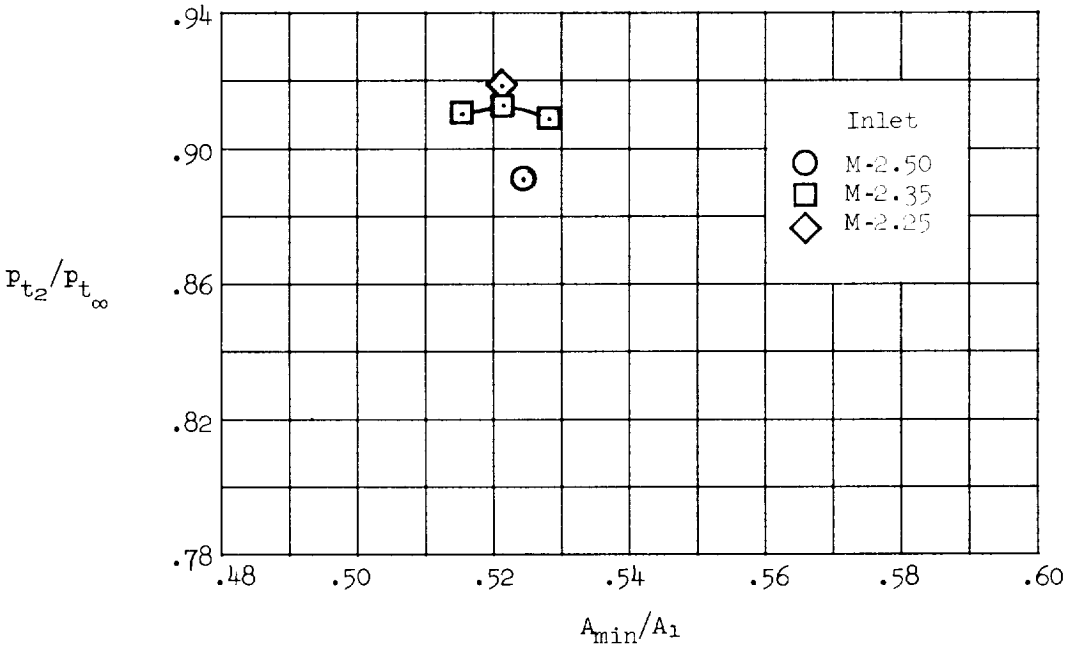

(b) Optimum boundary-layer bleed.

Figure 9.- Average total-pressure recovery at duct station 2 as a function of contraction ratio at M_∞=2.35; α=0°.

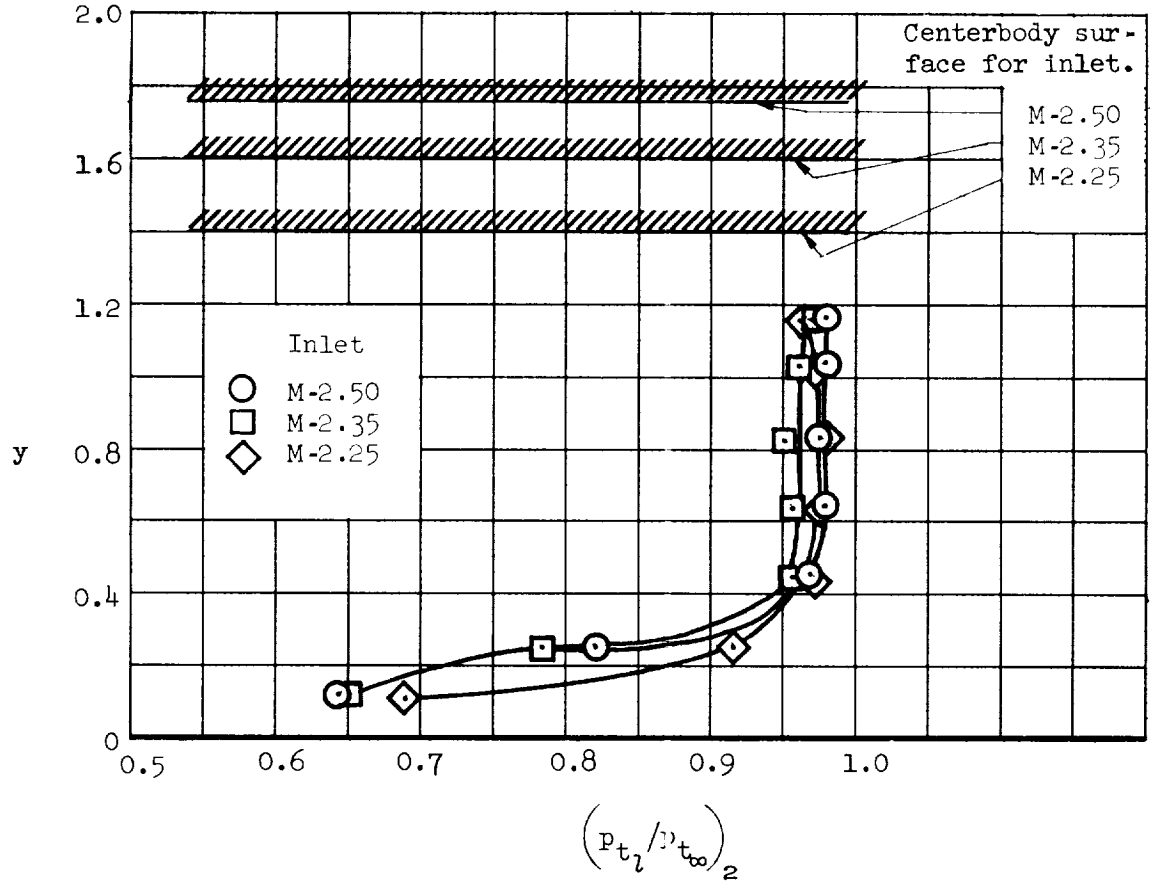

(a) No boundary-layer bleed.

Figure 10.- Total-pressure-ratio distribution between centerbody and annulus surface at duct station 2; centerbody position, x/r, near position for maximum pressure recovery; M_∞=2.35, α=0°.

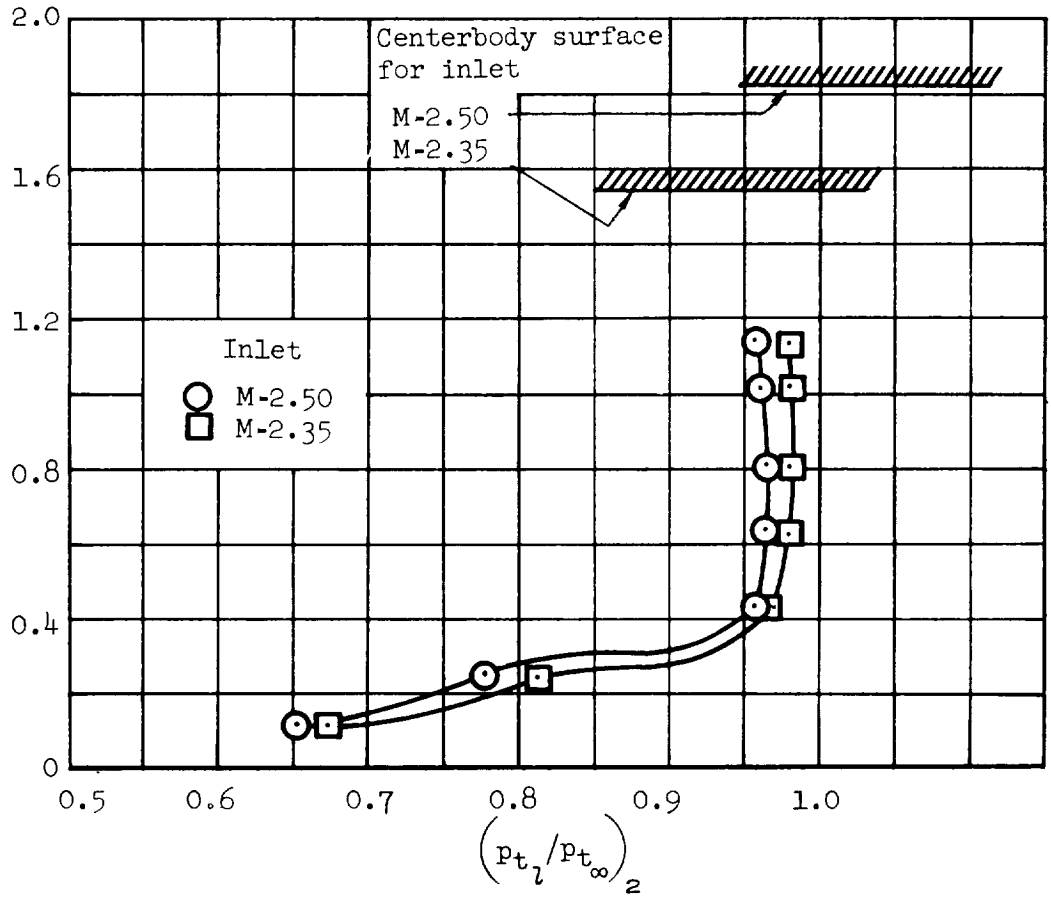

(b) Optimum boundary-layer bleed.

Figure 10.- Concluded.

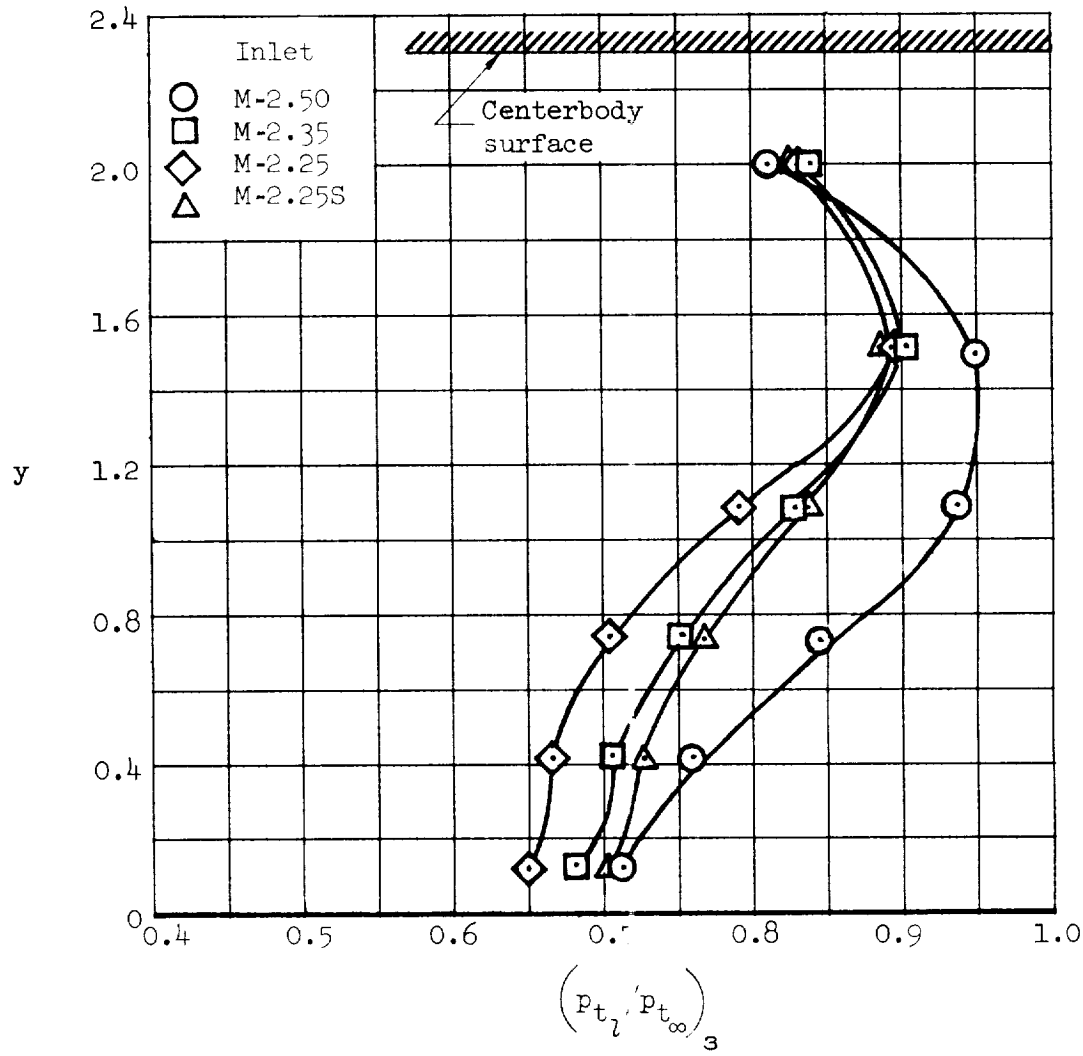

(a) No boundary-layer bleed.

Figure 11.- Total-pressure-ratio distribution between centerbody and annulus surface at duct station 3 at optimum inlet operating conditions; M_∞=2.35, α=0°.

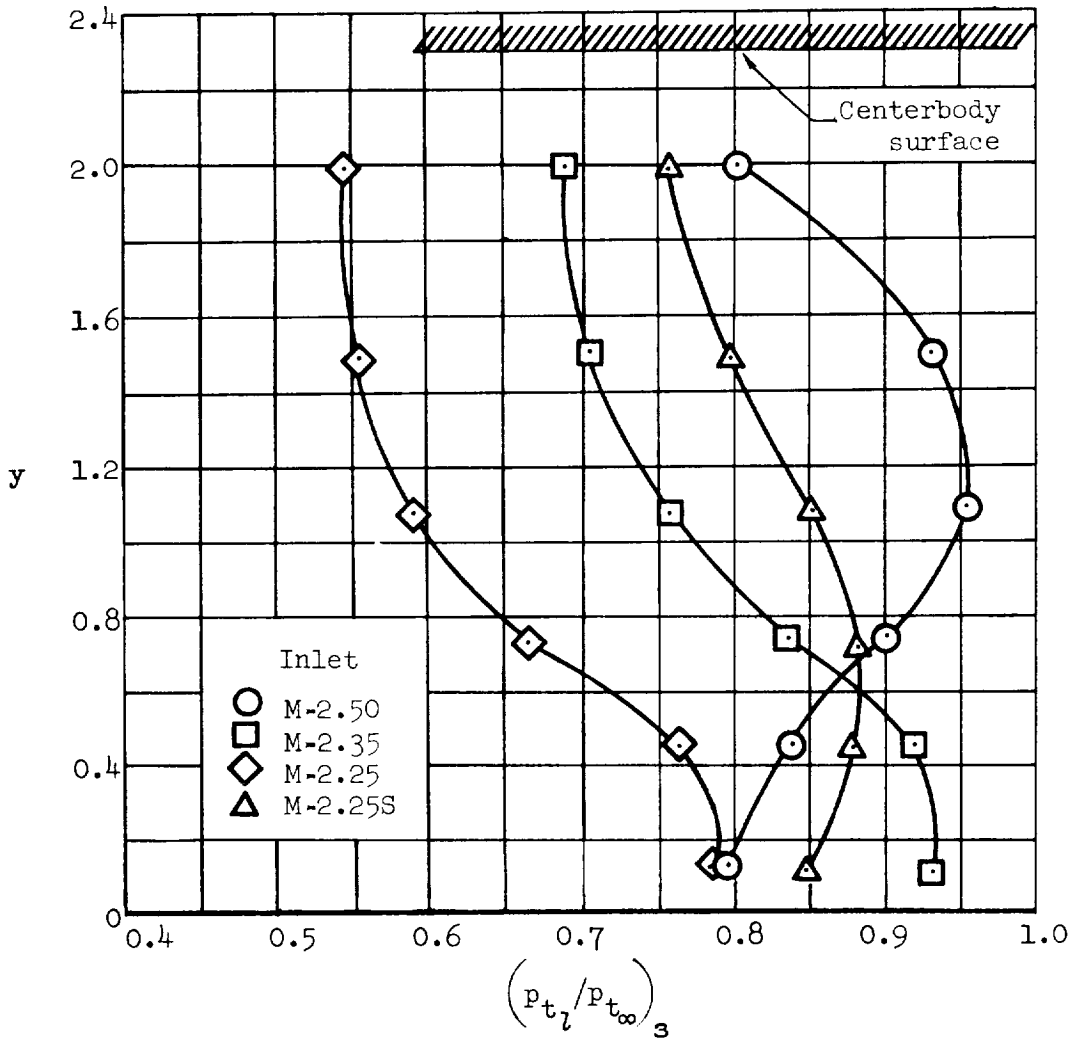

(b) Optimum boundary-layer bleed.

Figure 11.- Concluded.

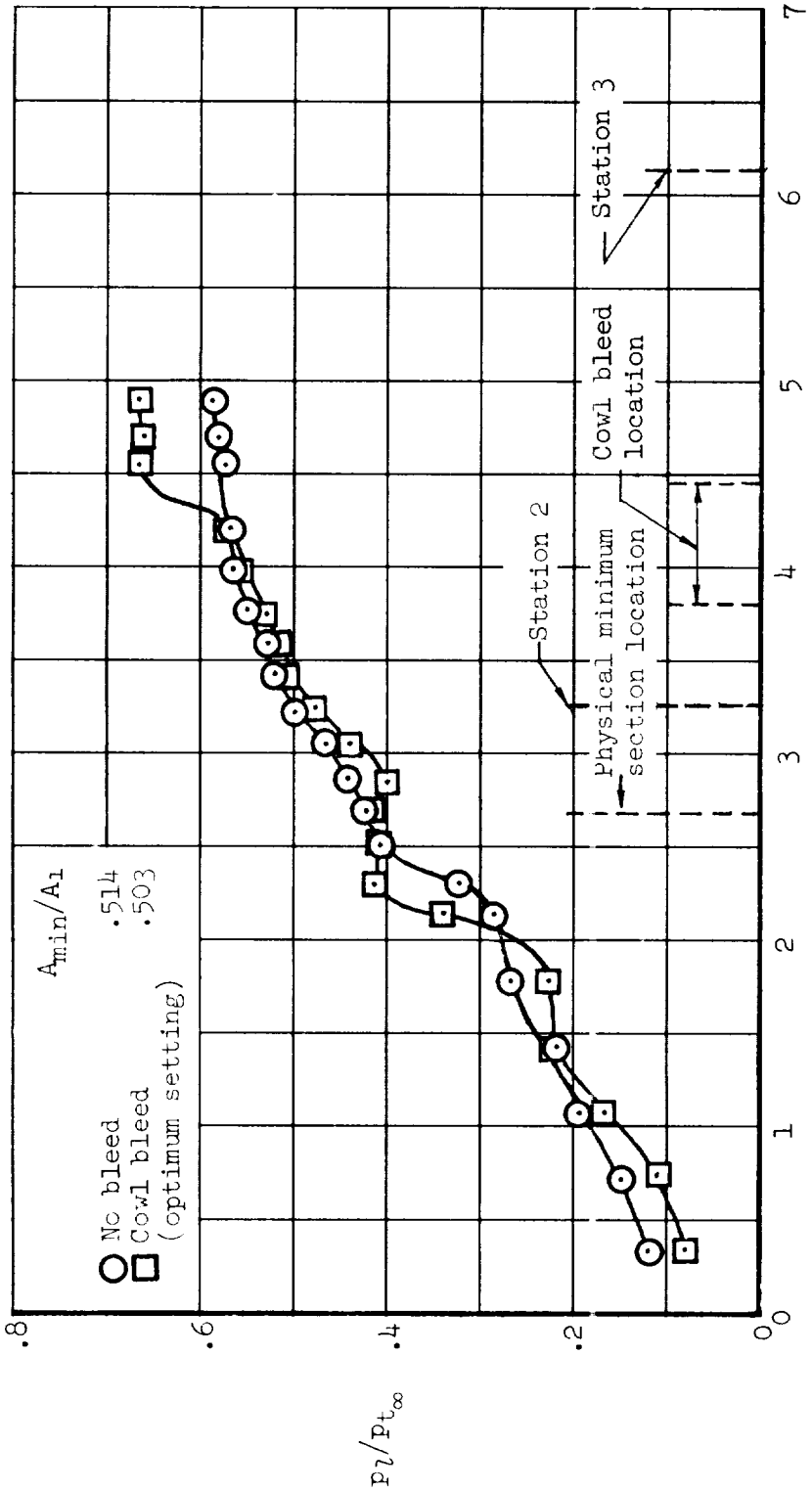

(a) Inlet M-2.50.

Figure 12.- Static-pressure-ratio distribution along the cowl of the various inlets at contraction ratios for maximum total-pressure recovery; M_∞=2.35, α=0°.

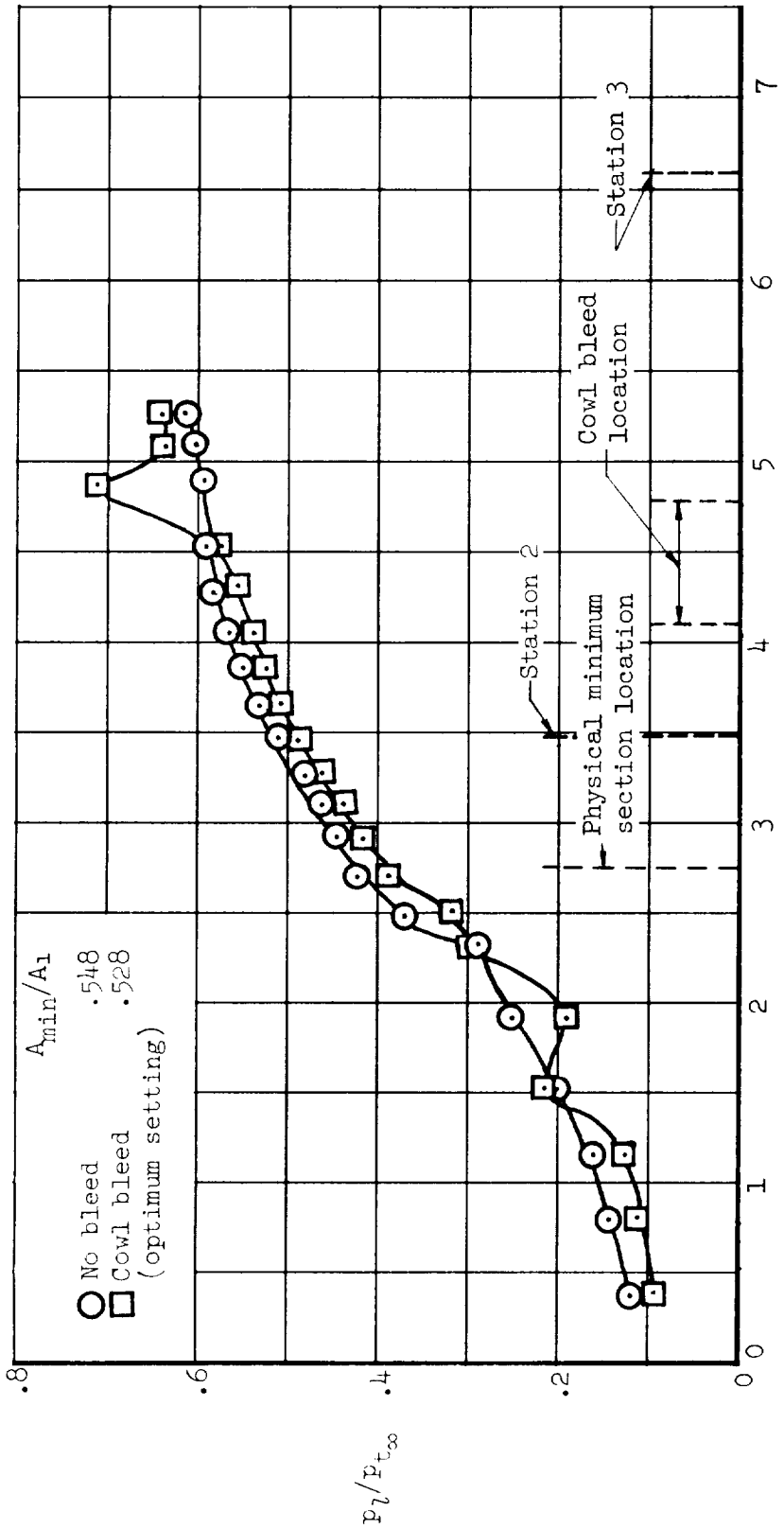

(b) Inlet M-2.35.

Figure 12.- Continued.

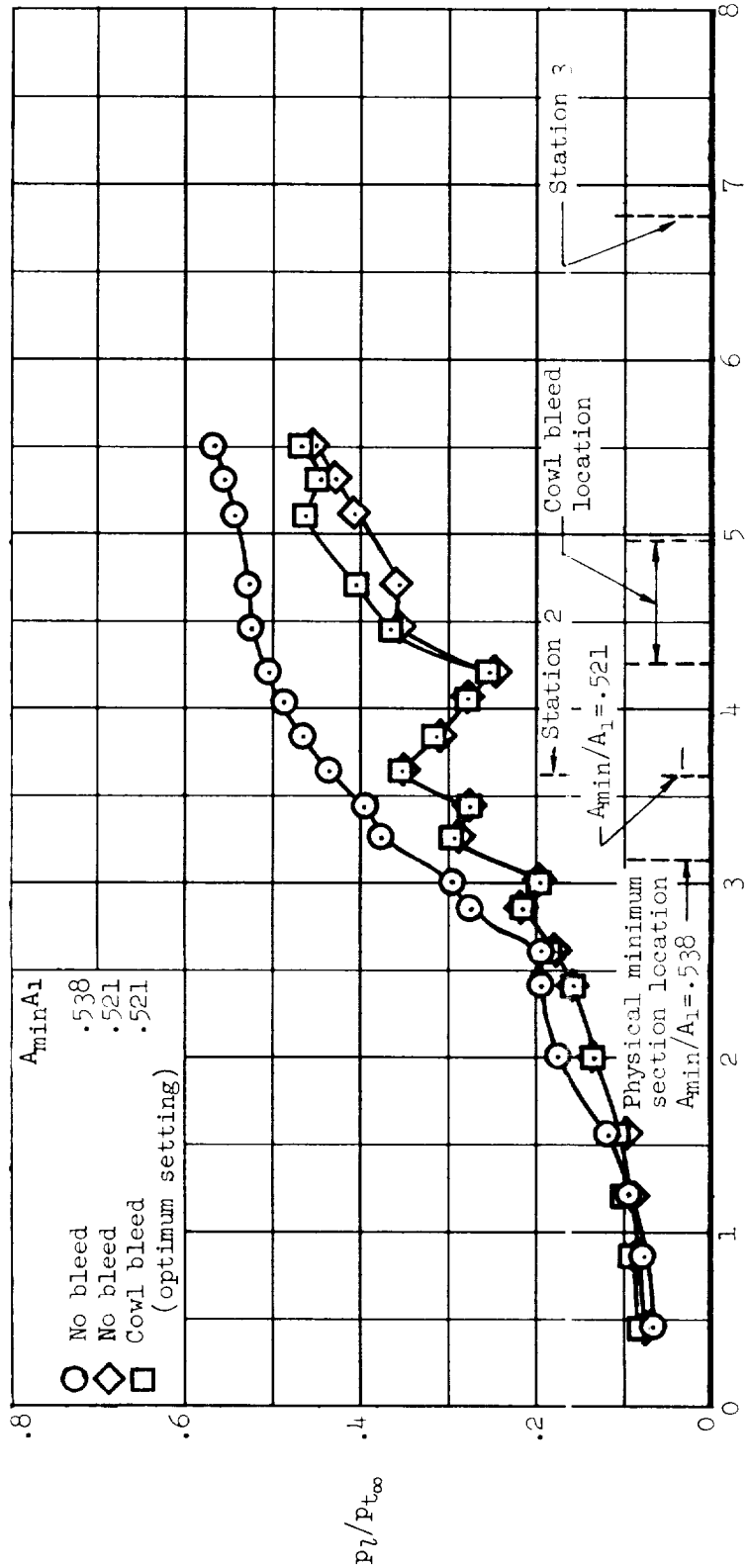

(c) Inlet M-2.25.

Figure 12.- Continued.

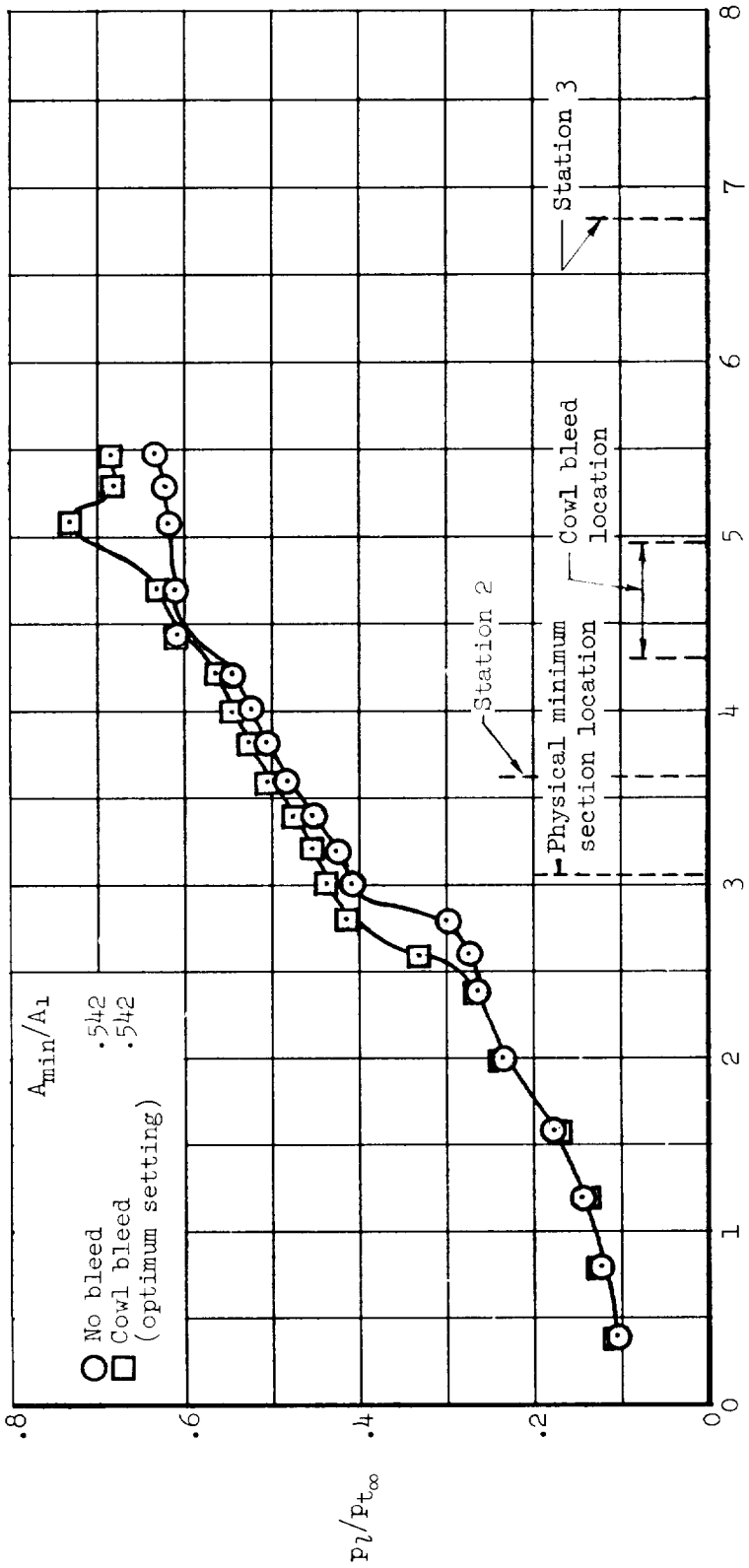

(d) Inlet M-2.25S.

Figure 12.- Concluded.

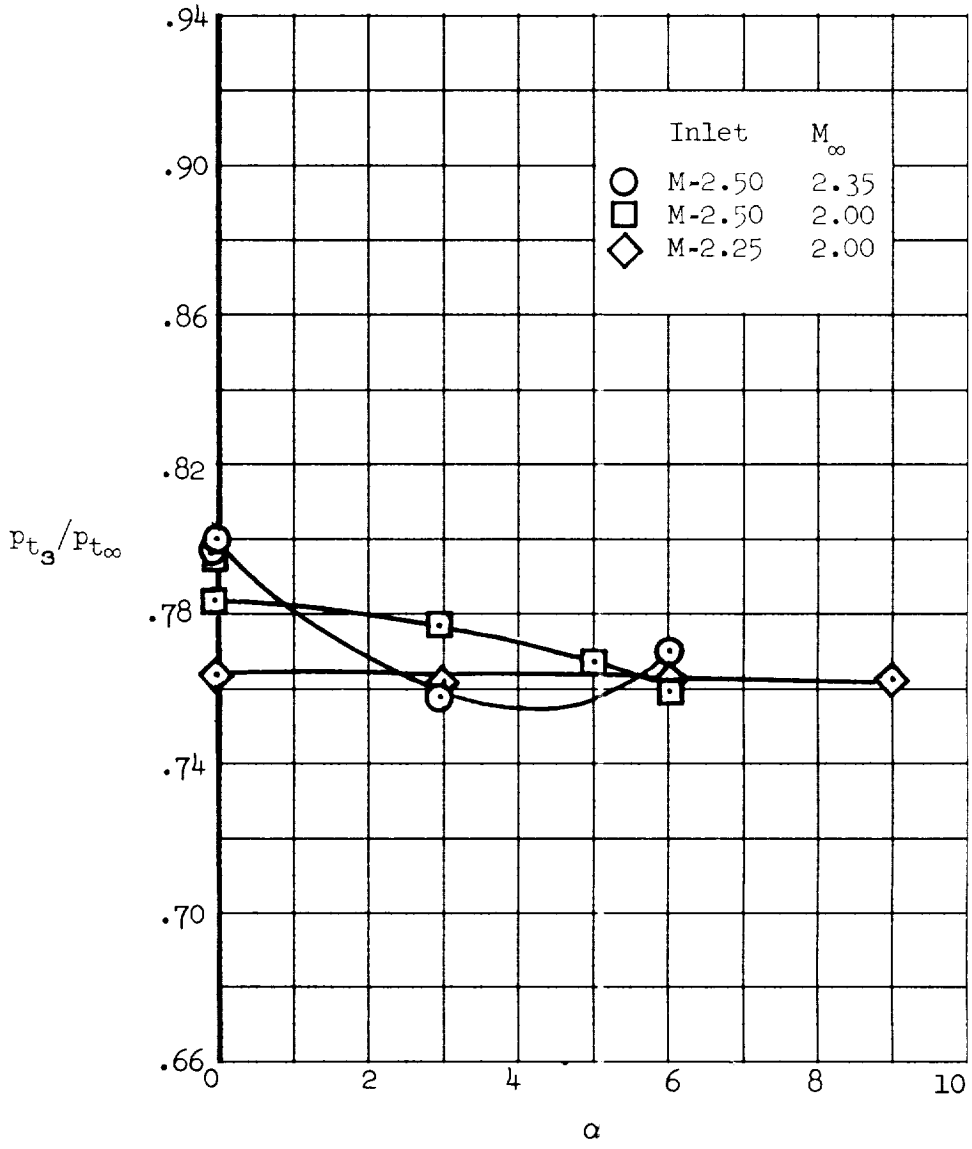

Figure 13.- Effect of angle of attack on total-pressure recovery at duct station 3; no boundary-layer bleed.

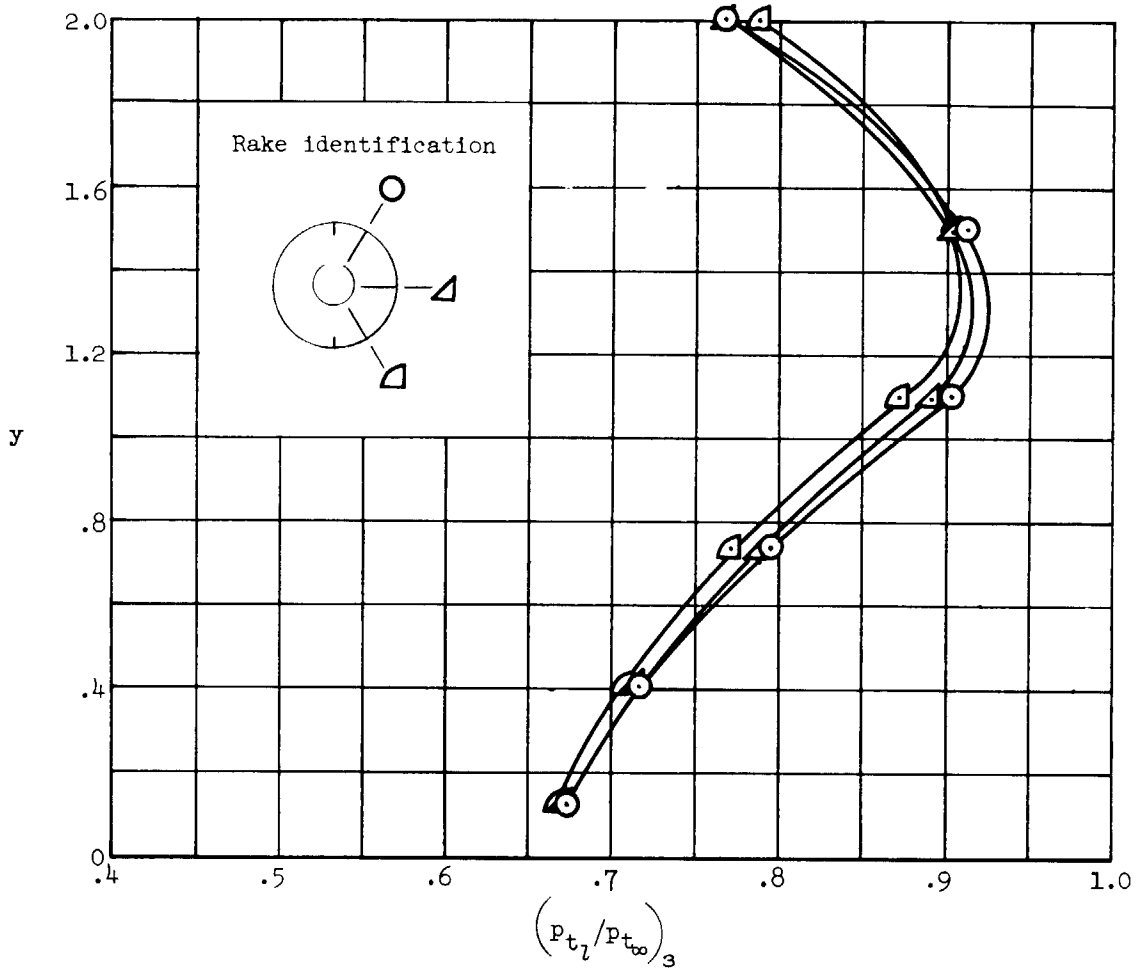

(a) $\alpha=0^{\circ}$.

Figure 14.- Total-pressure-ratio distribution between centerbody and annulus surface of inlet M-2.50 at duct station 3 for several angles of attack; $M_\infty = 2.35$, $A_{min}/A_1=0.536$.

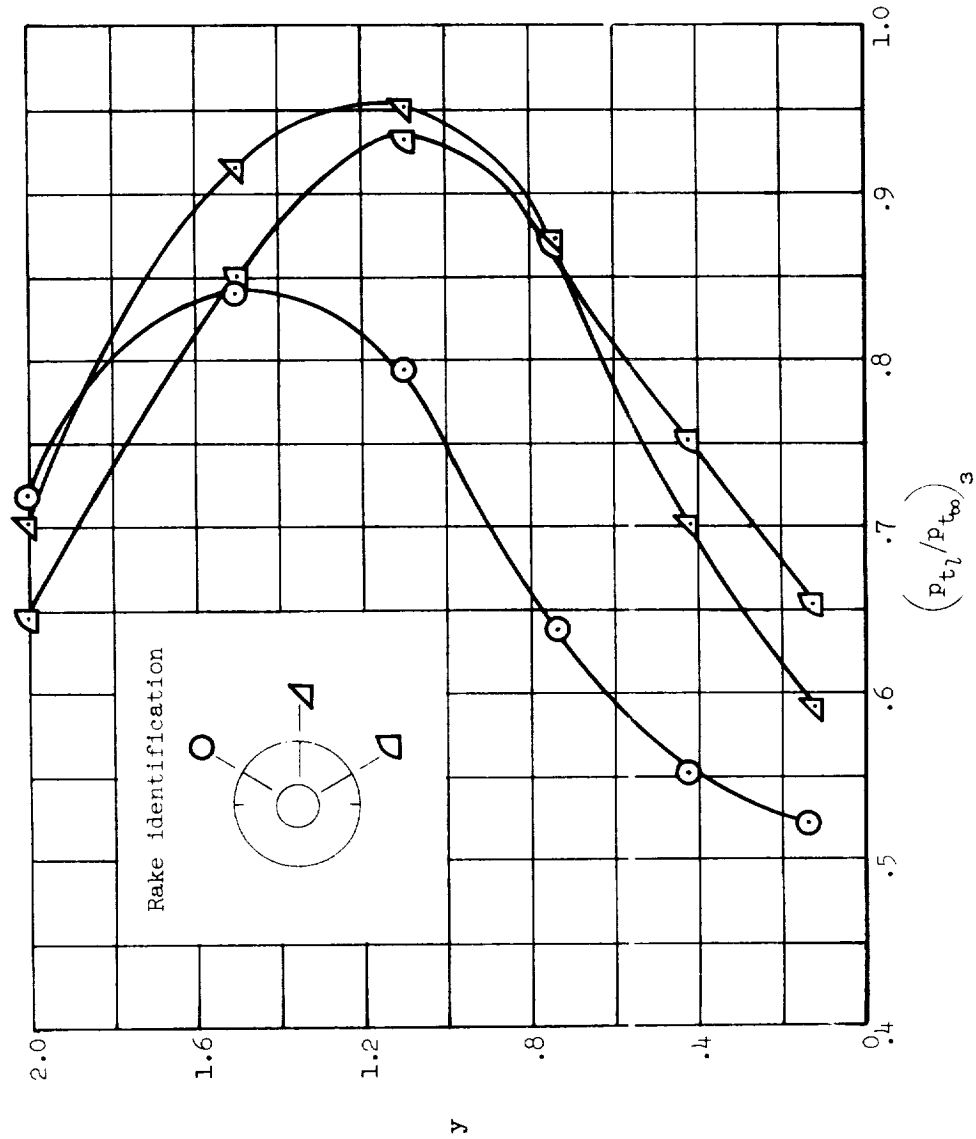

(b) $\alpha=3^\circ$.

Figure 14.- Continued.

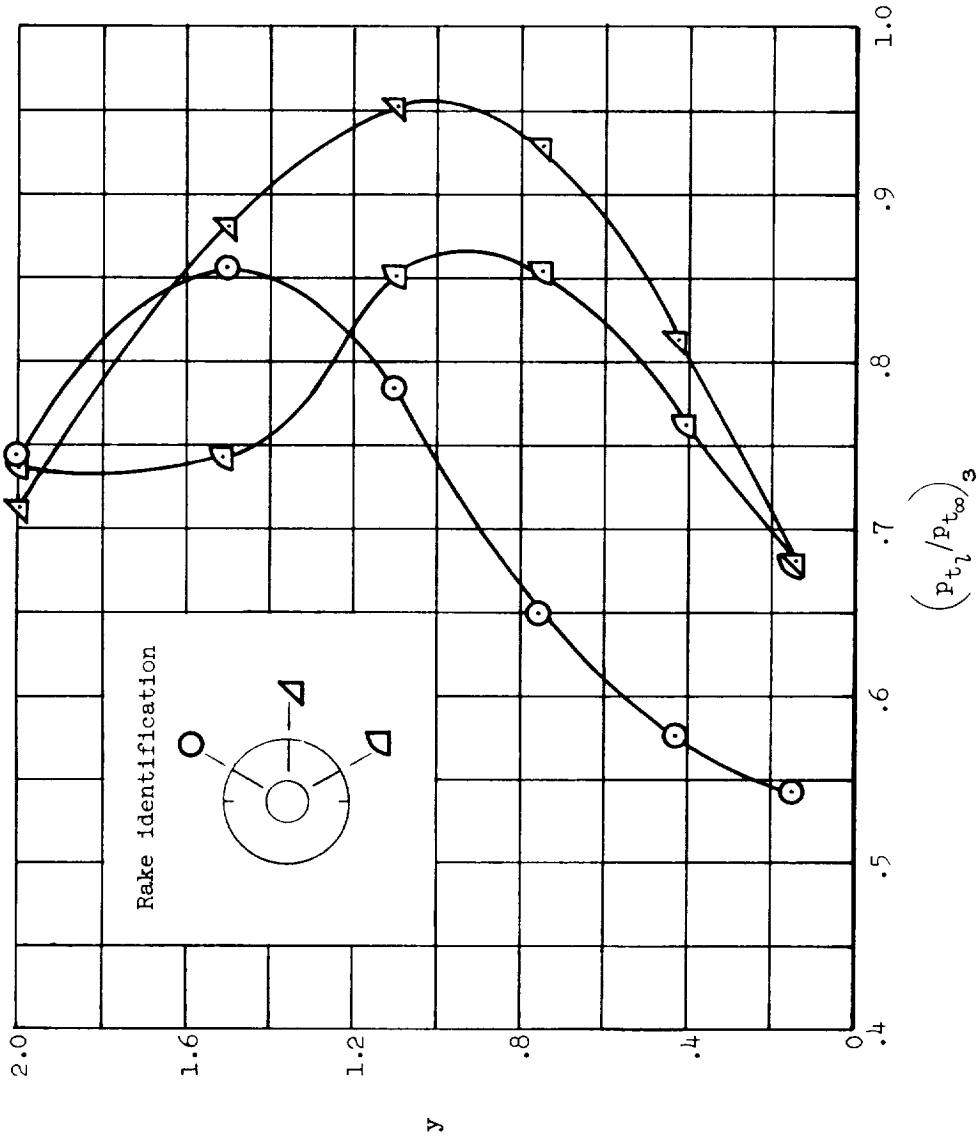

(c) $\alpha=6^\circ$.

Figure 14.- Concluded.

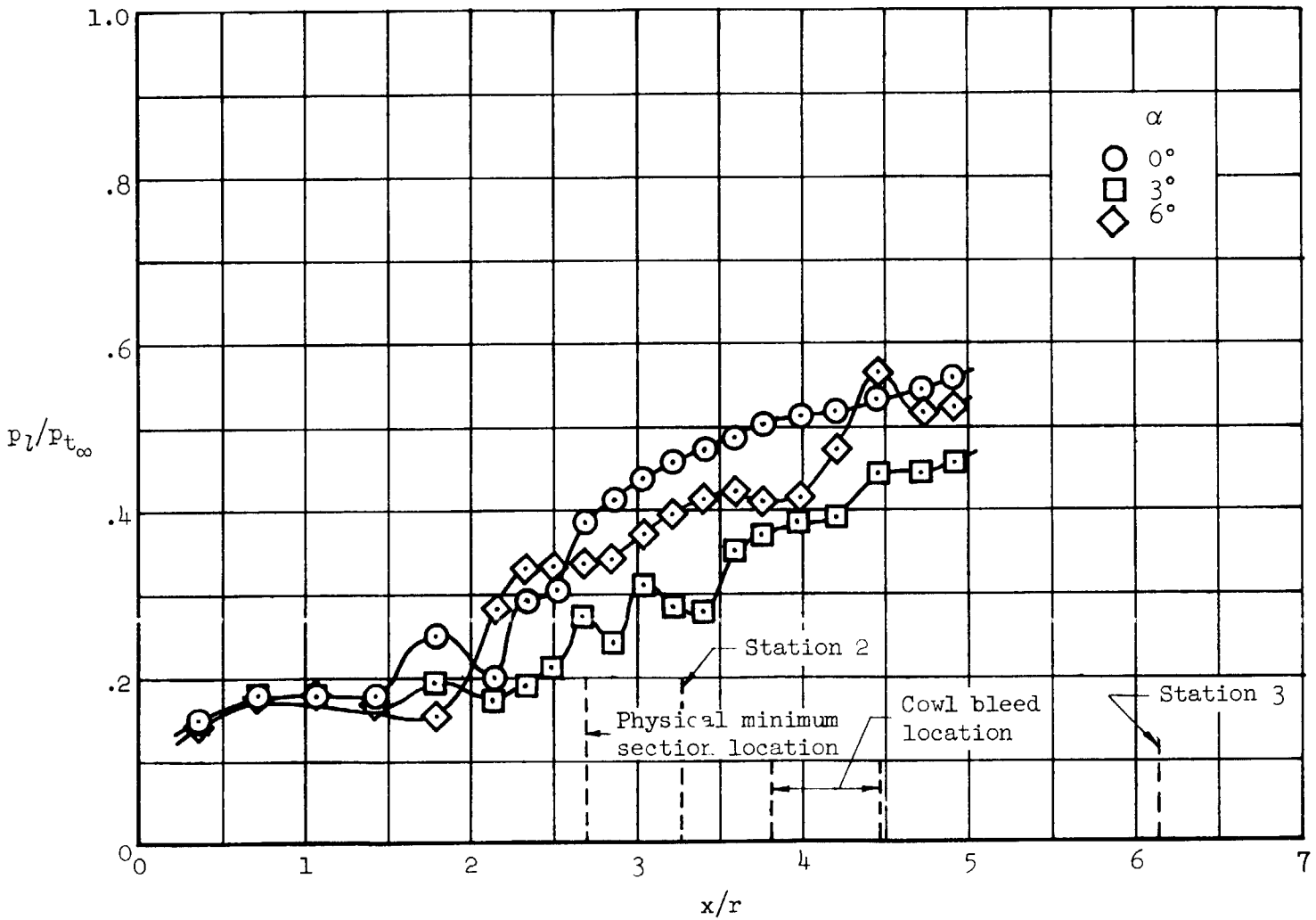

Figure 15.- Static-pressure-ratio distribution along the cowl of inlet M-2.50 for several angles of attack; M_∞=2.35; A_{min}/A_1=0.536.

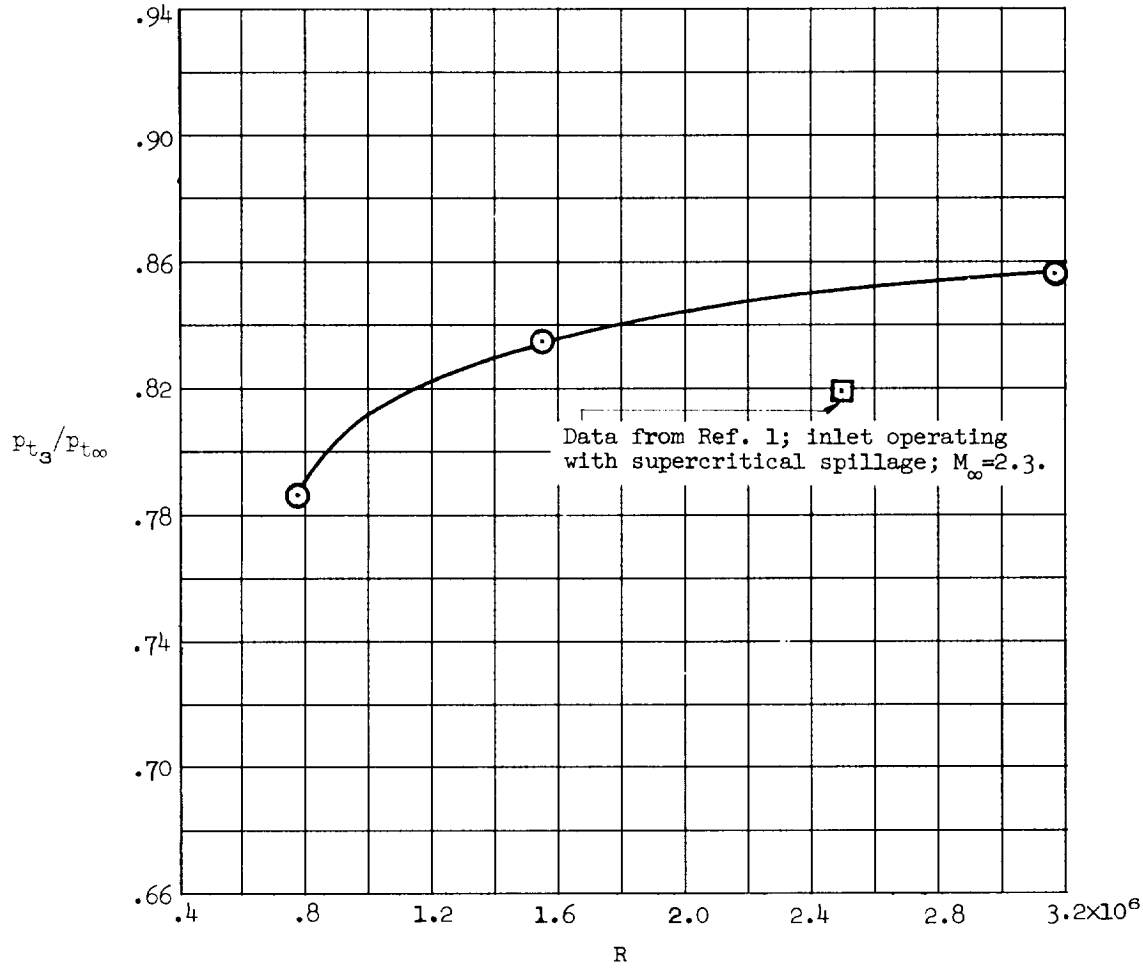

Figure 16.- Variation of pressure recovery with Reynolds number for inlet M-2.50; $\alpha=0^\circ$, M_∞= 2.35; no bleed.

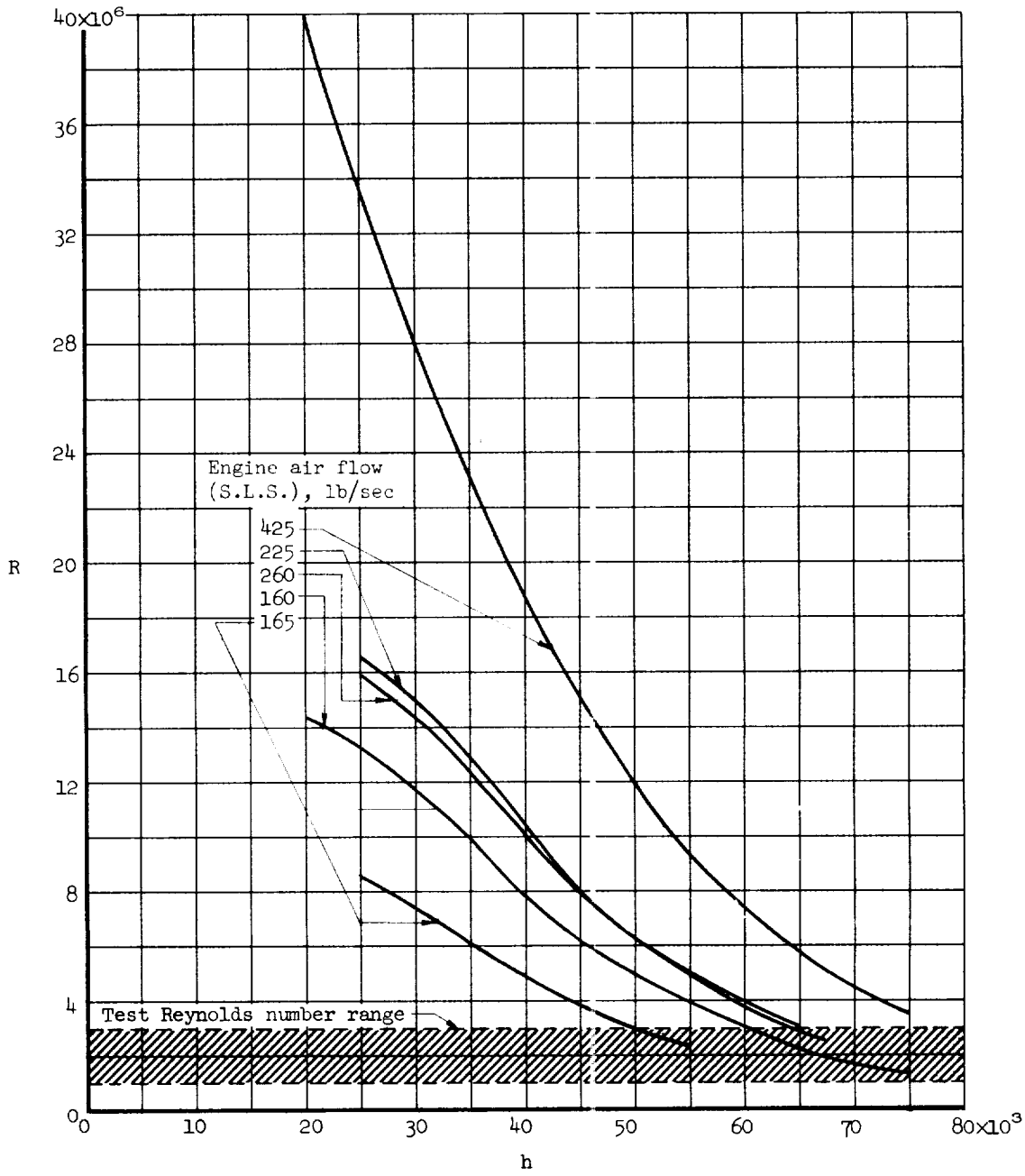

Figure 17.- Variation of flight Reynolds number with altitude for inlets sized to match certain engine maximum air flow requirements.

NOTES: (1) Reynolds number is based on the diameter of a circle with the same area as that of the capture area of the inlet.

(2) The symbol * denotes the occurrence of buzz.

Report and facility	Description			Test parameters				Test data				Performance		Remarks
	Configuration	Number of oblique shocks	Type of boundary-layer control	Free-stream Mach number	Reynolds number $\times 10^{-6}$	Angle of attack, deg	Angle of yaw, deg	Drag	Inlet-flow profile	Discharge-flow profile	Flow picture	Maximum total-pressure recovery	Mass-flow ratio	
NASA MEMO 12-31-58A Unitary 9- by 7-foot supersonic wind tunnel		Isen-tropic	Suction scoop	1.55 to 2.35	0.79 to 3.19	0 to 9	0	---	Yes	Yes	No	0.872	1.0	
NASA MEMO 12-31-58A Unitary 9- by 7-foot supersonic wind tunnel	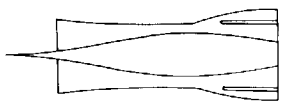	Isen-tropic	Suction scoop	1.55 to 2.35	0.79 to 3.19	0 to 9	0	---	Yes	Yes	No	0.872	1.0	
NASA MEMO 12-31-58A Unitary 9- by 7-foot supersonic wind tunnel		Isen-tropic	Suction scoop	1.55 to 2.35	0.79 to 3.19	0 to 9	0	---	Yes	Yes	No	0.872	1.0	
NASA MEMO 12-31-58A Unitary 9- by 7-foot supersonic wind tunnel		Isen-tropic	Suction scoop	1.55 to 2.35	0.79 to 3.19	0 to 9	0	---	Yes	Yes	No	0.872	1.0	

Bibliography

These strips are provided for the convenience of the reader and can be removed from this report to compile a bibliography of NASA inlet reports. This page is being added only to inlet reports and is on a trial basis.